ABSTRACT

Though the problem of wall streaking exists in all baseboard heaters, it is aggravated in case of electric baseboard heaters. It is postulated that the most important factor responsible for this is the higher temperature difference between the discharged air and the wall.

This study was undertaken to optimize the spacing of a fin element suitable for an electric baseboard heater to obtain maximum velocity for a minimum temperature of the discharged air. Higher discharged air velocity is desirable because it would help a properly designed heater enclosure to deflect the air away from the wall. Heat transfer from elements with a variable spacing to height ratio was studied and a study of some of the significant dimensions of the heater enclosure was also undertaken. A shadowgraph technique was used to study the air flow pattern induced by the various heater enclosures.

EXPERIMENTAL INVESTIGATION OF ELECTRIC BASEBOARD HEATERS

A Thesis Submitted

to

the Faculty of the Graduate Studies

The University of Manitoba

In Partial Fulfillment

of the Requirements for the Degree

Master of Science in Engineering (Mechanical)

by

Gopal Krishna Gupta

August 1968

ABSTRACT

Though the problem of wall streaking exists in all baseboard heaters, it is aggravated in case of electric baseboard heaters. It is postulated that the most important factor responsible for this is the higher temperature difference between the discharged air and the wall.

This study was undertaken to optimize the spacing of a fin element suitable for an electric baseboard heater to obtain maximum velocity for a minimum temperature of the discharged air. Higher discharged air velocity is desirable because it would help a properly designed heater enclosure to deflect the air away from the wall. Heat transfer from elements with a variable spacing to height ratio was studied and a study of some of the significant dimensions of the heater enclosure was also undertaken. A shadowgraph technique was used to study the air flow pattern induced by the various heater enclosures.

ACKNOWLEDGEMENT

The author wishes to express his sincere thanks to Professor R.E. Chant for his guidance and encouragement throughout the research program.

Thanks are also due to Dr. R.S. Azad and Professor D.W. Craik for their helpful suggestions, and to the technicians for their patience and help in constructing the experimental apparatus. Direct support received from National Research Council of Canada by means of an operating grant and financial and technical support received from Pioneer Electric Company Limited are also gratefully acknowledged.

TABLE OF CONTENTS

LIST OF FIGURES

NOMENCLATURE

SYMBOL	DEFINITION
q_v	Induced air flow rate to the fin assembly
T	Room temperature
ΔT	Temperature difference between the air leaving the fin assembly and room temperature
T_o	Fin base temperature
$\overline{T}$	Average fin temperature
T_w	Operating temperature of the probe
T_g	Ambient temperature of fluid
T_f	Film temperature
ρ	Air density
v	Velocity of air leaving the fin assembly
w	Velocity of fluid flowing over the probe
g	Acceleration due to gravity
C_p	Specific heat
Q	Power input to fin assembly
A	Heat transfer surface area
V	Voltage across the hot-wire probe.
V_o	Voltage across the hot-wire probe at zero fluid velocity
K	Thermal conductivity of fin material
μ	Absolute viscosity of air
ν	Kinematic viscosity of air
R_o	Cold resistance of the probe wire
R_w	Resistance of the probe wire at operating temperature.

R_g	Resistance of the probe wire at the ambient gas temperature
I	Current flowing through the probe
$\bar{H}$	Average convection coefficient
$\bar{h}A$	Convection conductance
S	Spacing between the fins
H	Height of the fin
l	Length of the probe wire
d	Diameter of the probe wire
D	Diameter of the calrod heater
t	Thickness of the fin
η	Efficiency of the fin
β	Coefficient of expansion for air

DIMENSIONLESS NUMBERS

N_{Gr}	Grashof Number -	$g\beta x^3(\Delta T)/\nu^2$
N_{Gz}	Graetz Number -	$(q_v \cdot \rho)\, C_p/K.H$
N_{Nu}	Nusselt Number -	$\bar{h}\, D/K$
N_{Pr}	Prandtl Number -	$\mu\, C_p/K$
N_{St}	Stanton Number -	$\bar{h}/C_p v \rho$

SUBSCRIPTS

f	Quantity evaluated at film temperature, T_f.
f'	Quantity evaluated at film temperature, $T_{f'}$
o	Properties evaluated at surface temperature

I. INTRODUCTION

The use of electric heating has been steadily increasing for the past several years and the most common form of residential electric heating system is electric baseboard heaters. This form of electric heating has certain inherent advantages such as individual room temperature control, safety of operation and versatility.

One of the disadvantages of using the electric baseboard heater is wall streaking; this is the development of stain pattern or the discoloration of the wall surface above the heater. The problem of wall streaking exists in all baseboard heaters regardless of the nature of the heat source. In the case of electric baseboard heaters, temperatures at the surface of the heating element as well as those of the discharged air are frequently higher than other systems using baseboard convectors. The higher temperatures aggravate the problem of wall streaking. Many other factors are deemed responsible for wall streaking including the temperature difference between the discharged air from the heater and the wall, contamination of room air and the design of heater enclosure. Wall streaking is a complicated process involving the interaction and combined effects of heat transfer, fluid flow and the dynamic behaviour of airborne particles and all the parameters affecting the wall streaking have not been analysed.

The most pertinent factor affecting the wall streaking caused by an electric baseboard heater was considered to be the higher temperature difference between the discharged air and the wall. The high temperature difference can be reduced by lowering the discharge air temperature from the heater. Such corrective action reduces the outlet velocity, but a high velocity is desirable for a properly designed heater enclosure can use the momentum inherent in the high velocity to deflect the air away from the wall. Thus the approach taken here was to experimentally investigate the effect of the fin spacing on the discharge velocity and temperature and to establish optimum conditions.

The changing of the spacing of the fins affects the heat transfer coefficient and although the effective use of the surface was not considered of paramount importance, it is significant. Thus heat transfer from the element was determined from measurements of the energy input to a heater. Measurement of temperature at the surface of the fin then permitted a study of the variation of the convective coefficients and the fin efficiency.

As indicated the heater enclosure plays a very important part in controlling the wall streaking from the baseboard heaters. The enclosure helps in deflecting the warm air away from the wall so that intermixing with the room air takes place before the warm air impinges on the wall. So a study of some of the significant dimensions of the heater enclosure was also undertaken.

A constant temperature anemometer was used to measure the low velocities involved in free convection. The hot wire probes were calibrated at low velocities in a varying temperature media. The technique used for calibrating the hot wire probes at higher temperatures was new and the development of the equipment forms part of this work.

II. LITERATURE REVIEW

II. 1. FREE CONVECTION FROM VERTICAL PLATE

Free convection from vertical plates was studied both experimentally and analytically by Schmidt and Beckman (1). For air having a Prandtl Number .74, the following equation was derived analytically

$$h_x = 0.360 \frac{K}{x} (N_{Gr})_x^{\frac{1}{4}}$$

Where h_x is the local convection coefficient.

Eckert and Jackson (2) and Eckert and Soehnghen (3) obtained photographs to illustrate important features of free convection from a vertical plate. A Machzehnder optical interferometer was used for these investigations. This instrument produces interference fringes which are recorded by a camera. The fringes are the result of density gradients caused by temperature gradient in gases. Temperature distribution near the plate were obtained from these photographs. Various available data on free convection from vertical plates have been correlated by McAdams (4).

The following formulas for values of $N_{Gr} \cdot N_{Pr}$ from 10^9 to 10^{12} is recommended by McAdams:

$$\frac{h_x L}{K_f} = 0.13 \left(\frac{L^3 \rho_f^2 g \beta_f \Delta T}{\mu_f^2} \cdot \left(\frac{C_p \mu}{K_f} \right)_f \right)^{\frac{1}{3}}$$

It may be noted that the convective coefficient is independant of "L", the height of the plate and depends only on the physical properties and the ΔT. Then for a gas with a small ΔT the equation may be simplified to the following form:

$$h_x = 0.19 (\Delta T)^{1/3}$$

which is for air at atmospheric pressure.

II. 2. FREE CONVECTION FROM PARALLEL PLATES

Many studies of free convection from vertical parallel plates are reported. Carpenter and Wassell (5) studied natural convection from parallel vertical plates in air. The convective heat loss per unit area was determined experimentally for parallel plates with various spacings and two different heights. The larger plates were each 5 feet x 4 feet and the smaller plates 5 feet x 1 ft. 4 in., the 5 feet dimension being horizontal in each case. The spacing between the plates was varied from ½ inch to 2½ inches. It was found that heat loss per unit area from parallel plates decreases when the spacing was reduced. The heat loss per unit area remained almost constant if spacing was increased above two inches. Also it was found that lower portions of plates were considerably more effective per unit area than the upper portions. The average heat loss per unit area was greater for shorter plates; the difference being greater at small spacings and small temperature excesses.

Elenbaas (6, 7) has done extensive work with channels and parallel plates on an experimental and analytical basis. He found out that $\bar{N}_{Nu}$ for the plates was a function of $\frac{S}{H} \cdot N_{Gr} \cdot N_{Pr}$. This was confirmed by plotting N_{Nu} as a function of $\frac{S}{H} \cdot N_{Gr} \cdot N_{Pr}$. An attempt was made to optimize the spacing between parallel plates at same uniform temperature. The results are discussed in the next chapter.

Ostrach (8) theoretically studied fully developed flow for free

convection between parallel plates. The surface temperatures of the plates were assumed to be constant but not necessarily equal. It was found that the flow and heat transfer from parallel plates, not only are functions of Prandtl and Grashof numbers but also depend on a dimensionless parameter $\frac{\beta g S}{c_p}$.

Bodoia and Osterle (9) studied free convection in a viscous fluid between heated vertical plates when the plates are not sufficiently high for fully developed flow to exist. The basic governing equations are expressed in finite difference form and solved numerically on a digital computer. Siegel and Norris (10) studied local heat transfer of long vertical plates. The space at the bottom and the sides was closed in most of the cases, but plates open at the bottom were also tested. It was found that if the bottom space was open, the closing of the sides did not have much effect on the heat transfer from the plates.

The work reviewed indicated that the heat flux decreased with $\frac{S}{H}$ for the range of spacing studied and that short plate without fully developed flow were more effective.

II. 3. FREE CONVECTION FROM FINS

Extended surfaces have been the subject of many extensive theoretical and experimental investigations. Murray (11) studied the annular fin of uniform thickness using the concept of fin effectiveness and assuming the convection coefficient over the fin as constant. Heat transfer from a single annular fin has been calculated using heat balance on the elemental particle on the fin. Effect of more than one fin has not been discussed. Gardner (12) investigated many shapes of fins and developed expressions for the fin efficiency. Weiner, Gross and Paschkis (13) studied circular finned cylinder and tested them in a water tunnel. Temperature distribution and variation of convection coefficient over the fins have been plotted. It was found that an approximate method of calculating heat flow based on average convection coefficient gives reasonably accurate results. Edwards and Chaddok (14) developed expression for a circular fin on tube configuration suitable for a relatively large spacing. Knudsen and Pan (15) studied tubes with essentially isothermal fins and correlated the results for his experiments.

Starner and McManus (16) experimentally investigated the heat transfer from base mounted rectangular fin arrays. Variation of convection coefficient for various fin spacing to height ratios were plotted. Figure 1 shows the variation of average convection coefficient as a function of the difference between the base and ambient temperatures with the base horizontal. It is interesting to note that set No. 3 shows the

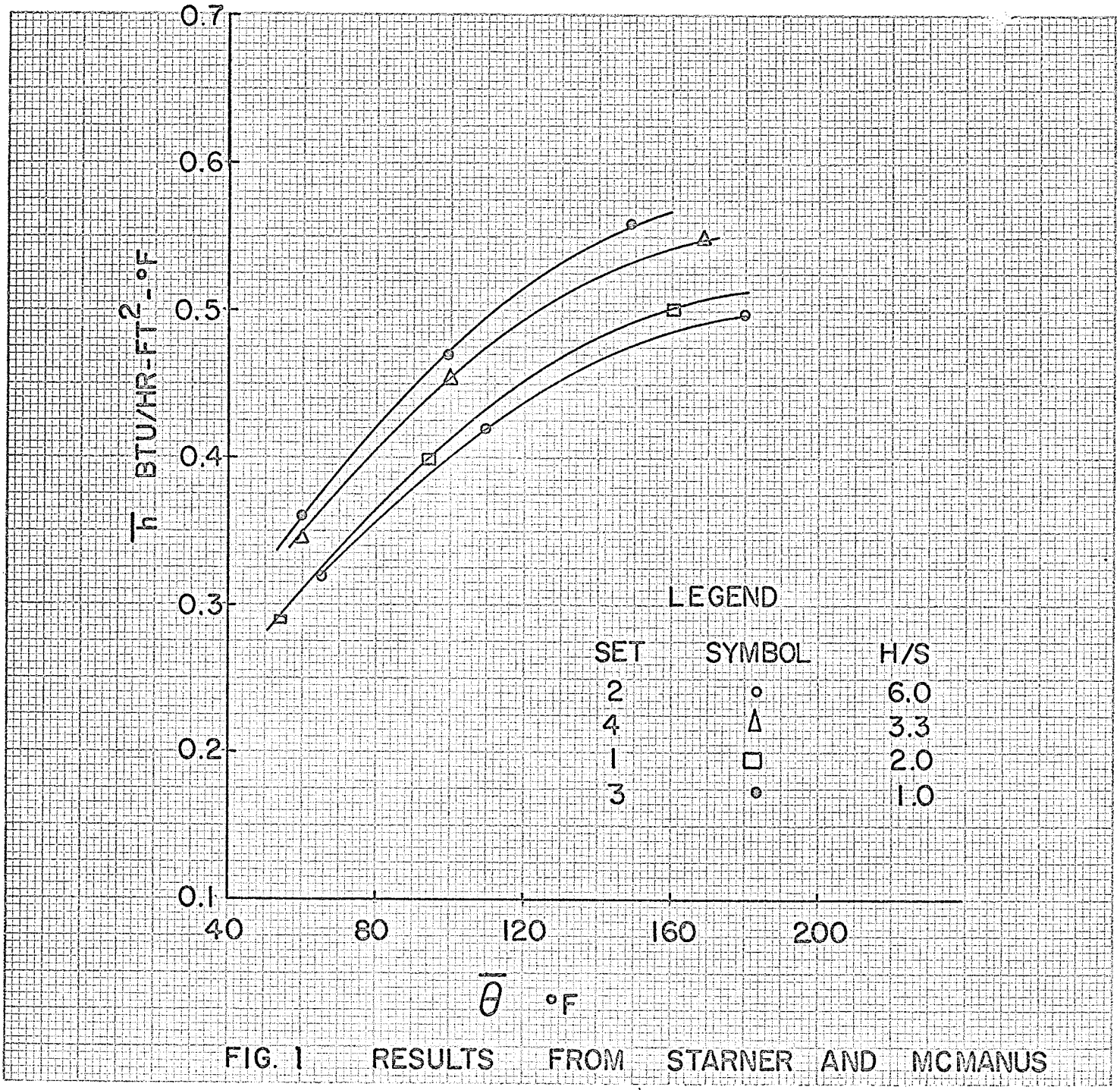

FIG. 1 RESULTS FROM STARNER AND MCMANUS

highest coefficients due to its wide fin spacing and thus the least boundry layer interference. Comparing the other three sets it can be seen that set No. 4 gives a convection coefficient about 15 per cent higher than set No.1 although the $\frac{S}{H}$ is lower. The authors contribute the higher values of the convection coefficient for set No. 4 to the higher absolute spacing which is 0.313 inches as compared to 0.250 inches for set No. 1. It also indicates that the parameter $\frac{S}{H}$ is inadequate to analyse the results varying both the height and spacing of the fins. Welling and Wooldridge (17) also studied rectangular fins. Both spacing and height of the fins were varied and it was shown that an optimum value of the $\frac{H}{S}$ ratio exists, above and below which free convection heat transfer would decrease. Harahap and McManus (18) continued the investigation of Starner and McManus (16) on base mounted fins and investigated the flow patterns above the fins. The flow patterns observed showed a pronounced chimney effect. The tallest fins possessed a well defined flow field with the flow of air entering the open ends of the fins and developing the pronounced vertical velocity components as the length of the fin was traversed. With the lowering of the fin height, the single chimney broke into several smaller chimneys. The data obtained for the horizontal orientation of the fins were generalised and the following correlation obtained:

$$(N_{Nu})_{L,o} = 5.22 \times 10^{-3} \left[(N_{Gr})_{L,o} (N_{Pr})_{o} \frac{S}{H} \right]^{0.570} \left(\frac{H}{L} \right)^{0.656} \left(\frac{S}{H} \right)^{0.412}$$

For $$10^{6} < (N_{Gr})_{L,o} (N_{Pr})_{o} \frac{S}{H} \leq 2.5 \times 10^{7}$$

and,
$$(N_{Nu})_{L,o} = 2.787 \times 10^{-3} \left[(N_{Gr})_{L,o} (N_{Pr})_o \frac{Sn}{H} \right]^{0.745} \left(\frac{H}{L} \right)^{0.656} \left(\frac{S}{L} \right)^{0.412}$$

for
$$2.5 \times 10^{7} < (N_{Gr})_{L,o} (N_{Pr})_o \frac{Sn}{H} < 1.5 \times 10^{8}$$

The product, Sn (n being the total number of fins), is essentially the width and thus doesn't in reality contribute to an understanding of the problem. The problem of optimizing the fin spacing to height ratio for maximum heat transfer has also been studied by a few others. As already indicated Elenbaas (6) solved the problem in case of uniform temperatures. Fairbanks and Marks (19) have used Elenbaas's results and allowed for the fin temperature variation by means of fin efficiency. This method is discussed in the next chapter.

II. 4. WALL STREAKING FROM BASEBOARD HEATERS

Wall streaking from electric baseboard heaters has been studied at Illinois Institute of Technology Research Institute (20). A specially designed test room was used to relate the performance of various electric baseboard heaters under controlled environment. The test room was maintained at a temperature of approximately 75°F. The atmosphere in the test room was polluted artificially by introducing carbonaceous dust, wool lint and smoke generated by hot fat. Relative wall streaking characteristics of the heaters were determined by measuring the change in reflectance of initially uniform panels that were hung on the wall above the heaters. Shadowgraphs which show the airflow pattern above each heater were recorded by means of photographs and photographs of the exposed panels were also taken. All the experimental data obtained has been presented in the form of graphs and photographs, but no effort was made to analyse the results.

Wall streaking has also been studied at the Battelle Memorial Institute (21). A review of the literature pertinent to the problem is presented. The findings of the literature review have been reported under three headings: Dirt Staining of Walls, Dust in Room Air and Thermal Forces on Aerosol Particles. It has been concluded from the review that thermal forces on the dust particles may contribute significantly to the deposition rate on the wall. These thermal forces act in conjunction with, and are partly controlled by, the flow pattern of the air as it

leaves the heater. An experimental study on various baseboard heaters confirmed the conclusions drawn from the literature review. Variations in heater enclosure design were also investigated for a simple experimental heater. The heaters were tested in a controlled environment test room. The deposition rates on a controlled temperature wall for various airborne materials were determined. The experiments indicated that wall discoloration increases with power input to a heater, concentration of the test aerosol in the room and temperature gradient at the test wall. It was found that in normal conditions air flow pattern is more important than the temperature gradient. Also it was found that electric baseboard heaters do not contribute to electrostatic deposition of charged particles nor do they cause wall discoloration by capture and decomposition of lint which may normally be found airborne in a home. The deposition rate on the wall decreased with an increase in the heater height and thickness (distance from the wall to top outlet). It was also found that the design of heating element may be of considerable importance in controlling the wall discoloration. A restriction to air flow by the heater element was found to result in increased deposition on the wall.

Baljet (22) has studied the design of electric baseboard heater to decrease the wall streaking. A finned heater element has been used but no details of the heater element design have been given. A heater enclosure has been designed to decrease wall streaking. The front and back deflecting panels of the enclosure help in directing the stream of warm air away from the wall for effective mixing with room air. Another

feature of the design is that the cooling fins cannot be touched through the warm air outlet. Ventilated air spaces have been provided between the baffles and the enclosure which contribute to very low external surface temperature of the baseboard heater and also provide a good location for a thermal protection device.

The wall streaking studies reviewed show that the mechanism of wall streaking and thus the exact effect of various parameters on wall streaking are not yet known. While others are studying the effect of various contaminants, the present investigation is to study the effect of $\frac{S}{H}$ on the outlet temperature and velocity, both of which affect the wall streaking of an electric baseboard heater. The tendency of the discharged air to deflect towards the wall has been explained. Also some dimensions of the heater enclosure were studied to determine the effect on the flow pattern above the heater.

III. THEORETICAL CONSIDERATIONS

III. 1. FREE CONVECTION FROM A VERTICAL PLATE

If a heated vertical plate is placed in a cold fluid, the fluid in its immediate neighborhood experiences an increase in its temperature as a result of heat transfer from the plate and begins to flow in an upward direction. Thus a boundary layer arises with zero thickness at the lower edge and with an increasing thickness in the upward direction. Within the boundary layer, the temperature decreases from the value on the plate surface to the uniform value which the fluid has outside the heated region. The velocity of the fluid varies from zero at the plate and then increases to a maximum value and then decreases to zero at the edge of the boundary layer.

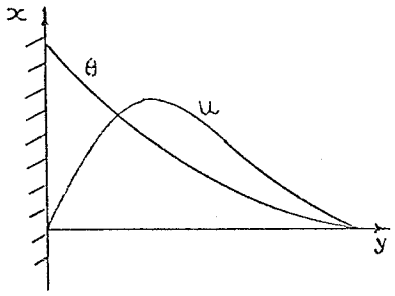

Figure 2.

Taking the distance along the plate surface from the lower edge x, and the normal distance from the plate surface y; the governing equations are:

$$\frac{\partial u}{\partial x} + \frac{\partial v}{\partial y} = 0$$

$$u \frac{\partial T}{\partial x} + v \frac{\partial T}{\partial y} = k \frac{\partial^2 T}{\partial y^2}$$

$$u \frac{\partial u}{\partial x} + v \frac{\partial u}{\partial y} = \nu \frac{\partial^2 u}{\partial y^2} + g \left(\frac{T - T_\infty}{T_\infty} \right)$$

provided that the temperature difference between the wall and the air is small as compared with the absolute temperature. Let the undisturbed air temperature be T_∞, and the temperature of the plate be T_1. T is the temperature at any point and u and v are velocities in x and y directions respectively, then let

$$\theta = \frac{T - T_\infty}{T_1 - T_\infty}$$

The boundary conditions are:

$$u = v = 0 \quad , \quad \theta = 1 \quad at \quad y = 0 \; ;$$

$$u = 0 \quad , \quad \theta = 0 \quad at \quad y = \infty$$

These equations can now be transformed into ordinary differential equations by suitable substitutions (23). The ordinary differential equations have been solved for air by Pohlhausen and the theoretical local value of the Nusselt Number at the point distance x from the lower edge of the plate was found to be

$$(N_{Nu})_x = 0.359 \, (N_{Gr})_x^{\frac{1}{4}} \quad . \; . \; . \; . \quad 3.1$$

where $$(N_{Nu})_x = \frac{h x}{k}$$

and $$(N_{Gr})_x = \frac{g \beta x^3 (T_1 - T_0)}{\nu^2}$$

III. 2. FREE CONVECTION FROM PARALLEL VERTICAL PLATES

Parallel plates at uniform temperatures were analysed by Elenbaas (6) to find the optimum spacing between the plates to dissipate maximum amount of heat for a given base area. The following relation was recommended.

$$\frac{S_{opt}}{H} \left(N_{Gr}\right)_{S_{opt}} \left(N_{Pr}\right) \doteqdot 50 \quad . \quad . \quad . \quad . \quad 3.2$$

Where the constant was determined experimentally. This equation can be expressed for air as follows:

$$S_{opt} \doteqdot 2.9 \left(\frac{H\, T_\infty}{g\, \Delta T}\right)^{\frac{1}{4}} \left(\frac{\mu}{\rho}\right)^{\frac{1}{2}} \quad . \quad . \quad . \quad 3.3$$

This expression is for parallel plates at uniform temperatures and so can only be used as an approximation for rectangular fin tube geometry.

III. 3. FREE CONVECTION FROM FINS

An analytical solution of a single circular fin on a tube is available (11), but for square fins even the case of a single fin on a tube has not been analysed due to complicated boundary conditions. Fairbanks and Marks (19) used Elenbaas (6) curves, Figure 3, which were plotted from Equation 3.2, to determine S from an optimum value of thickness of the fin (t). Fin efficiency was used to allow for the fin temperature variation. The heat transferred from the surface area, A, is given by

$$Q = h A \Delta T = h A \eta \Delta T_b \quad \ldots \quad 3.4$$

Where Q is the heat transferred through the fin surface area A, and ΔT_b is the difference between the tube temperature and the ambient air temperature. Substitutions are made for the values of fin efficiency, surface area and convection coefficient in Equation 3.4.

Elenbaas (6) has shown that at the optimum spacing, for infinitely long parallel plates at uniform temperatures, the Nusselt Number ($\frac{h S}{K}$), is approximately 1.2. Fairbank and Marks assumed that this value of Nusselt Number should also hold for the fin-tube geometry. The convection coefficient can now be isolated from Equation 3.4 and the heat transferred from the fins expressed as in the following equation.

$$Q = f (H , D , S , t , K , K_t , \Delta T_b) \quad \ldots \quad 3.5$$

This equation is complicated and is difficult to solve for the maximum value of heat transfer. An iteration procedure has been used to calculate the optimum geometry of the fins. First values for D and t are assumed. Then for a given value of ΔT_D, a first approximation for S is obtained from Figure 3. which has been plotted from Elenbaas (6). Now h is calculated assuming the Nusselt number to be 1.2 and efficiency of the fin is calculated from circular fin relationships by using an average outer diameter of the fin. The new value for $\Delta T = \eta \Delta T_D$ is calculated and the procedure is repeated until a limiting value for the fin efficiency is reached. Heat transfer from the fins can now be calculated. The procedure is repeated for other values of t . Thus Q as a function of the thickness of the fin is obtained for the assumed value of D . The optimum value of the thickness is then the value which gives the maximum heat transfer. The spacing can now be calculated.

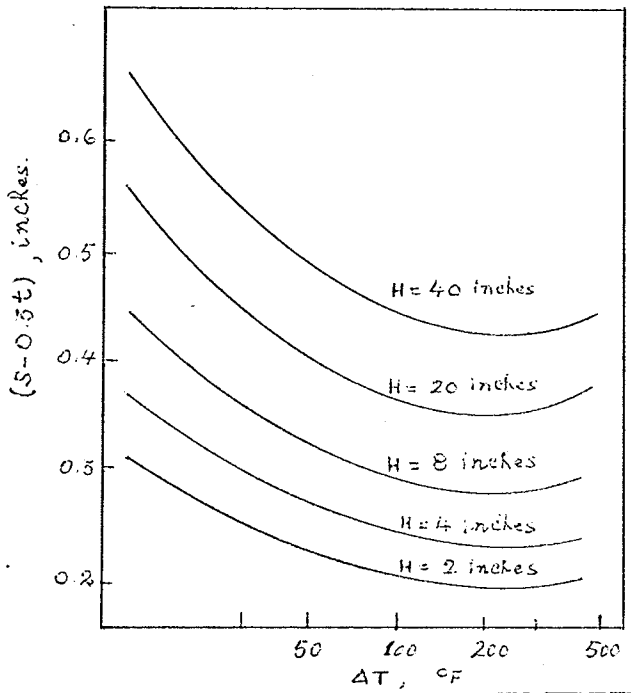

FIGURE 3. OPTIMUM SPACING FOR UNIFORM FIN TEMPERATURE.

An attempt was made to check the accuracy of the method used by Fairbank and Marks (19) on the basis of the results obtained from the present investigation. (For details see Chapter VI).

III. 4. DIMENSIONAL ANALYSIS

To determine the governing parameters for the present problem, a dimensional analysis was carried out. The procedure from Langhaar (24) was followed and the following equation was obtained: (For details see Appendix A)

$$N_{Nu} = A(N_{Gz})^{m}(N_{Gr})^{n}(N_{St})^{p}(N_{Pr})^{q}(\Delta T.\beta)^{r}\left(\frac{H g \beta}{C_p}\right)^{x}\left(\frac{S}{H}\right)^{y}\left(\frac{\Delta T}{\Delta T_p}\right)^{z} \quad \ldots . \quad 3.6$$

This equation indicates the parameters which are used in the present investigation. No attempt, however, was made to evaluate the constants in the equation with the experimental results.

Two dimensionless parameters, N_{Gz} and ($\Delta T.\beta$), obtained above are used frequently in analysing the results. Graetz Number, N_{Gz}, represents the induced mass flow rate and $\Delta T.\beta$ is the potential causing the mass flow rate.

IV. OUTLINE OF EXPERIMENTAL APPROACH AND CALIBRATION OF HOT-WIRE ANEMOMETER

IV. 1. GENERAL REMARKS

The literature review shows that extensive work has been done on free convection from single vertical plates and parallel vertical plates. In most of the cases the plates were maintained at a uniform temperature. Rectangular fin arrays have been studied experimentally and optimum values of $\frac{S}{H}$ have been obtained. A rectangular fin-tube geometry has been used in the present investigation and so these results are not applicable.

The undesirable phenomena of wall streaking, which occurs in approximately ten per cent of the installations, is affected by the flow pattern and by the discharge temperature of the convector. Thus a fin geometry which would yield a maximum velocity or momentum for a fixed outlet temperature is desirable. The other desirable feature of the geometry is the arrangement that will yield a satisfactory flow pattern. The purpose of this investigation was then to study the effect of the spacing on the ratio of the induced mass flow to the discharge air temperature, which controls the potential inducing the mass flow.

The work of other experimenters indicates the lack of data to support

optimization of the spacing of rectangular fins and the results obtained in this work will supplement existing data.

IV. 2. APPROACH OF THIS WORK

To study the heat transfer characteristics of the fins, the variation of induced air flow and the temperature of the discharged air from the fin element, the following measurements were taken for the various fin geometries:

(1) Power input to the fin element.

(2) Fin surface temperatures.

(3) Amount of air induced by the fin element.

(4) Temperature of air discharged by the fin element.

(5) Velocity of air discharged for few fin geometries.

Also to study the effect of various dimensions of the baseboard heater enclosure shadowgraph photographs of the air flow induced by the various enclosures were taken.

IV. 3. CONSTANT TEMPERATURE HOT-WIRE ANEMOMETER

The probe of the hot-wire anemometer consists of a fine electrically heated wire stretched across the ends of two prongs. When exposed to an air stream the wire loses heat by convection and the energy input required to maintain the constant temperature is a function of the velocity. The velocity is determined from the measured value of current or voltage. The variation of current with the velocity of the air stream is established by calibration tests. This calibration characteristic of the probe is subject to change, partly through the "ageing" of the wire and partly through the accumulation of dust, which affect the thermal conditions at the wire surface. Thus hot-wire probes must be frequently calibrated.

The hot-wire probes have been extensively used for measurement of velocity of air and other fluids at room temperature, and so the nature of calibration curve in such cases is known. However no studies using hot-wire probes to measure velocity of a varying temperature media have been reported. So equipment to calibrate the hot-wire probes at low velocities in a varying temperature was designed and fabricated and the nature of the calibration curves studied.

IV. 4. CALIBRATION EQUIPMENT

The design of the calibration equipment was adapted from a set up suggested by Almquist and Legath (28) for measurement of low velocity flow. The details of the apparatus are shown in Figures 4 and 5. It consisted of a tank with an inflow of water whose pressure was kept constant by a pressure regulator. Keeping the water pressure constant was important, because any variation in the pressure would change the amount of water flowing into the tank which in turn would affect the air velocity from the tube. The air displaced by the inflowing water was fed through a drier to remove excess moisture. The air from the drier was passed through the heater and the temperature of the air could be controlled by changing the power input to the heater. Finally the air was passed through a 5/16 inch diameter tube 2 feet long, and the probes were positioned on the centre line at the outlet. The tube was long enough to ensure fully developed flow. The volume flow of air was taken equal to the volume of water flowing into the tank which was determined by timing the change in level. An important feature of this equipment was that low velocities could be measured accurately.

The accuracy depended upon the pressure regulation of the water, the measurement of rate of level change, the temperature of the air and the position of the hot-wire probe at the tube outlet. The accuracy of the pressure regulator valve was stated to be ± 2% by the manufacturer. Assuming the water pressure varied sufficiently to warrant the use of the

valve, the error in the water flow due to this pressure variation would be ± 1%. Repeated timings of a constant water inlet flow showed that results were reproducible with a limit of ± 2.5%. Therefore the accuracy of the rate of change of the level measurement and thus the air flow out of the tank was taken to be ± 2.5%.

The outlet temperature was measured by a thermocouple and manual balancing potentiometer with a resolution of ± 1°F. This introduced an average error of ± 0.5% in the temperature of air. The velocity profile at the outlet of the tube was ascertained to be parabolic by a traverse and a plot against the radius squared. This is shown in Figure 15. The mean velocity was then taken to be 0.5 times the maximum velocity which occurs at the centre. Accuracy was thus dependent upon the positioning of the probe. A vernier was used for the purpose and the probe was then re-positioned in an attempt to obtain the maximum reading. The vernier could be read to ± 0.001 inches and re-positioning showed a variation of point of maximum velocity to ± 0.003 inches. Because of parabolic shape of the velocity profile this introduced an error of less than 0.5%.

Therefore the maximum error of the velocity determination was taken to be 2.75%.

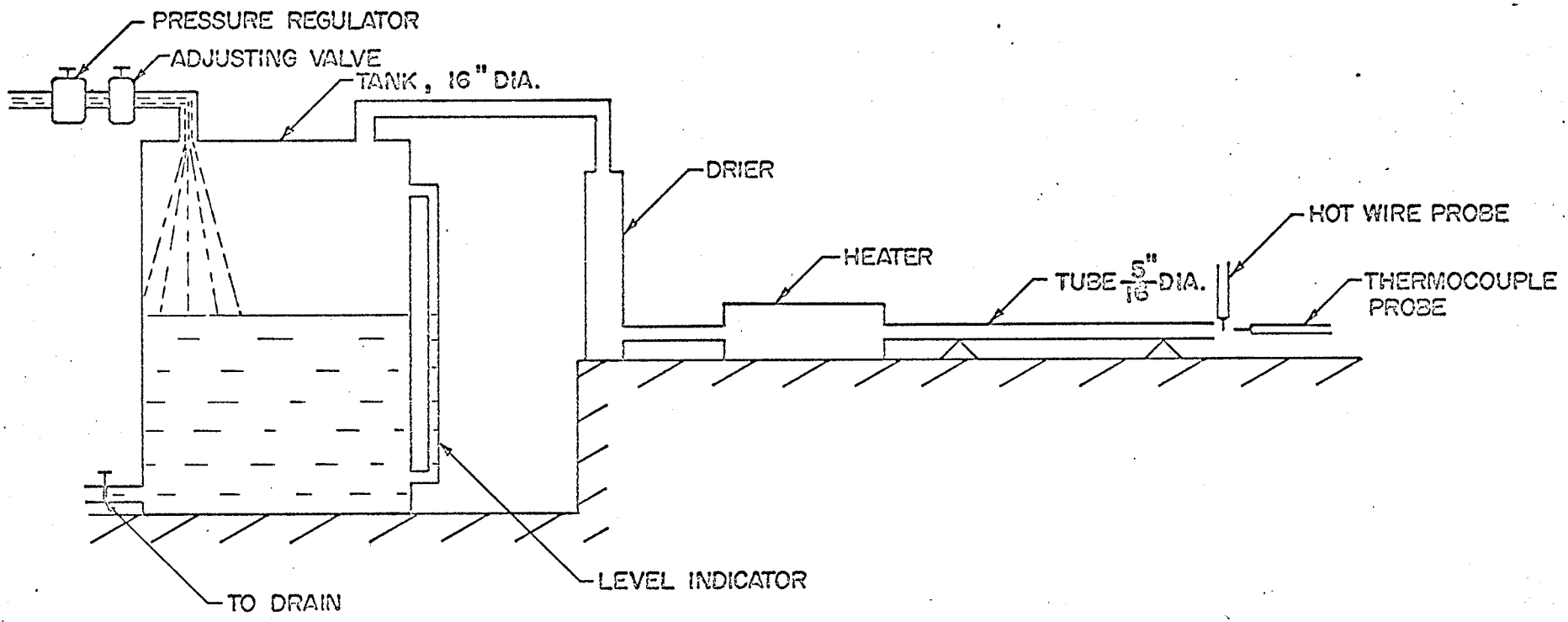

FIG. 4 HOT WIRE PROBE CALIBRATION SET-UP.

FIGURE 5

HOT WIRE PROBE CALIBRATION EQUIPMENT

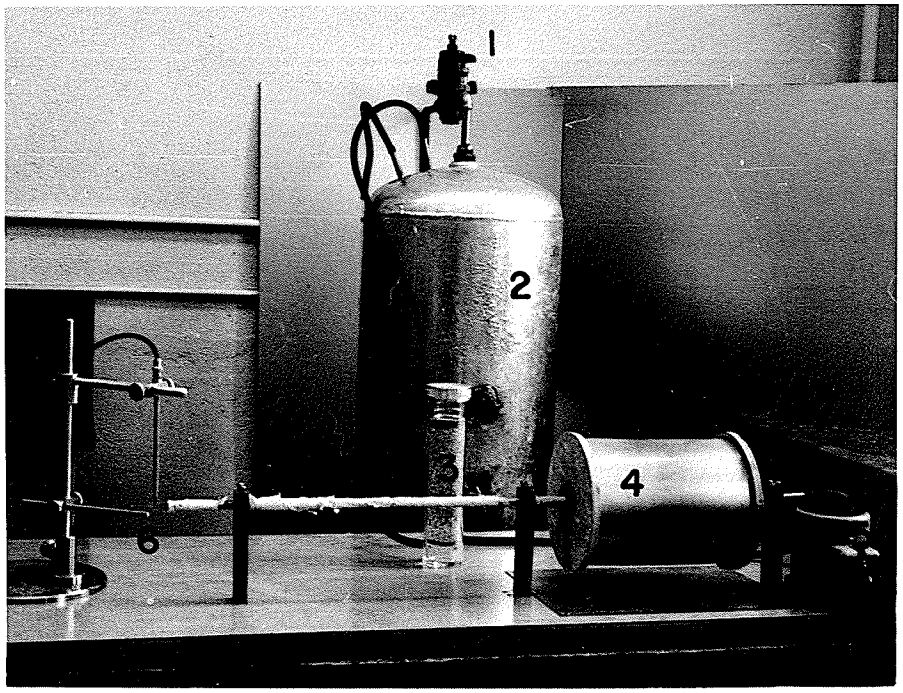

1. Pressure Regulator.
2. Tank.
3. Drier.
4. Heater.
5. Power Transformer.
6. Probes.

IV. 5. CALIBRATION RESULTS

Hot-wire probes were calibrated in air at four different constant velocities with temperature as the variable. Figure 16 shows the resulting calibration curves. It may be noted that calibration curves for different velocities meet at a point on the temperature axis. That means that at this temperature the heat loss from the probe is zero as no power is needed by the probe to keep its temperature constant. This could only happen if the temperature of the ambient air became equal to the probe temperature. Therefore the point where calibration curves meet was assumed to be the probe temperature.

It was not convenient to use Figure 16 to determine an unknown velocity. Another set of curves, shown in Figure 17, was therefore drawn from values obtained in Figure 16. V_o and V are the voltage required to keep the temperature of the probe constant at zero and 'w' velocity respectively. It may now be seen that the variation of $V^2 - V_o^2$ with $\sqrt{w}$ is linear. Now if the temperature of the flow and the voltage required by the probe is known, V_o can be read from Figure 16 and $\sqrt{w}$ can now be obtained from Figure 17. The velocity of the air flow can now be calculated.

IV. 6. RESPONSE EQUATIONS

For thermal equilibrium conditions of a constant temperature probe, the heat loss per unit time from the hot-wire of the probe must be equal to the heat generated per unit time by the electric current flowing through the wire.

Following the approach of Hinze (25), King's semi empirical equation for the heat loss from the probe wire can be written as

$$I^2 R_w = (A + B\sqrt{W})(T_w - T_g) \quad \ldots\ldots \quad 4.1$$

where

$$A = 0.42\, e\, \pi\, K_f\, \ell\, (N_{Re})_f^{0.20} \quad \ldots\ldots \quad 4.2$$

$$B = 0.57\, e\, \pi\, K_f\, \ell\, (N_{Re})^{0.33} \left(\frac{\rho_f\, d}{\mu_f}\right)^{0.50} \quad \ldots\ldots \quad 4.3$$

The term $A\,(T_w - T_g)$ represents heat loss due to free convection and radiation and $B\sqrt{W}\,(T_w - T_g)$ represents forced convection.

To find out the variations in the values of the constants 'A' and 'B', with a change in the temperature of the flowing fluid, two cases with different fluid temperatures have been considered. Let the value of the constants A and B be A_o and B_o when the temperature of the fluid changes from T_g' to T_g .

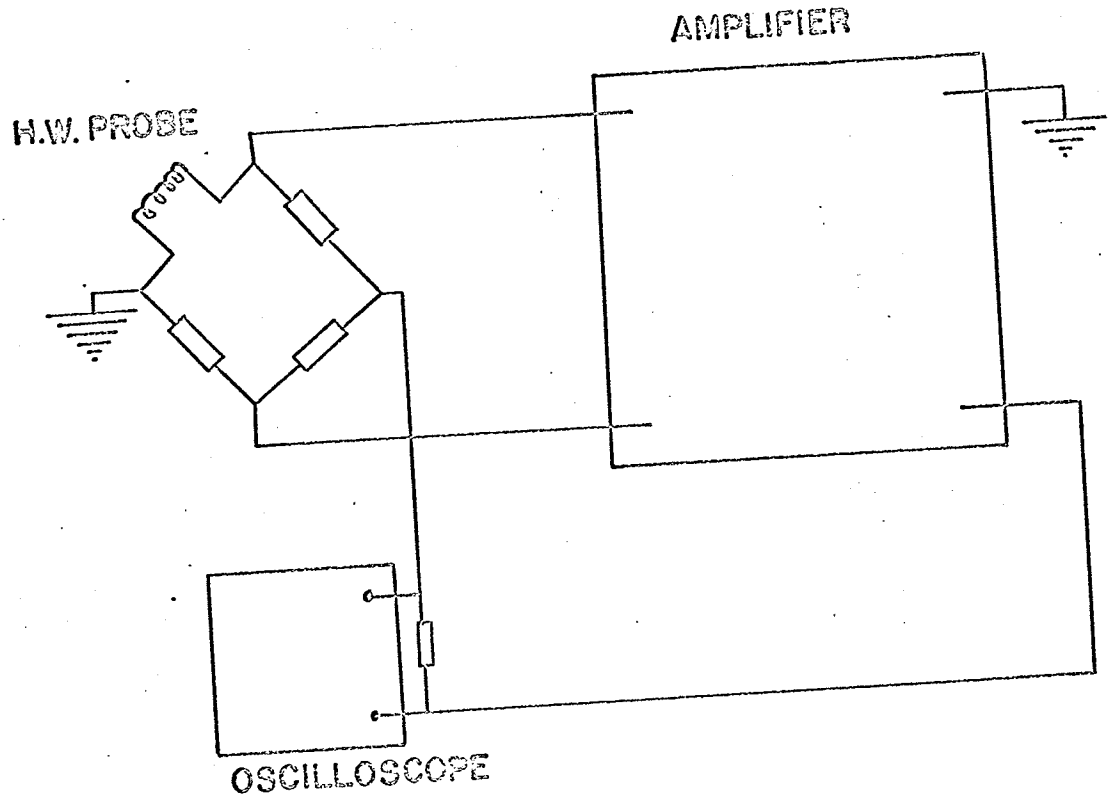

FIGURE 6 CONSTANT TEMPERATURE HOT WIRE ANEMOMETER

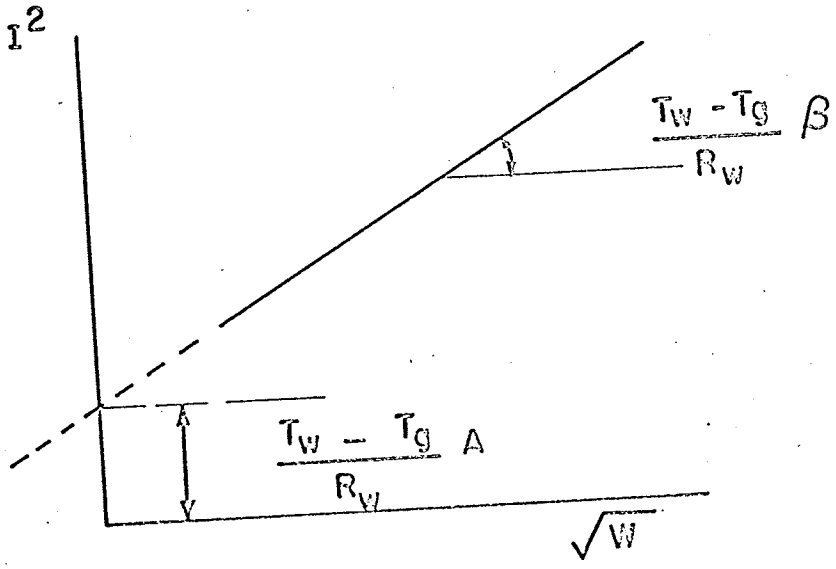

FIGURE 7 RELATIONSHIP BETWEEN I^2 AND $\sqrt{W}$

From Equation 4.2

$$\frac{A}{A_o} = \frac{K_{f'}}{K_f} \left(\frac{(N_{Re})_{f'}}{(N_{Re})_f} \right)^{0.20} \quad \ldots\ldots \quad 4.4$$

From Equation 4.3

$$\frac{B}{B_o} = \frac{K_{f'}}{K_f} \left(\frac{(N_{Re})_{f'}}{(N_{Re})_f} \right)^{0.33} \left(\frac{\rho_{f'} \mu_f}{\rho_f \mu_{f'}} \right)^{0.50} \quad \ldots\ldots \quad 4.5$$

As $\mu = \frac{K N_{Re}}{C_p}$,

$$\frac{\mu_f}{\mu_{f'}} = \frac{K_f}{K_{f'}} \cdot \frac{(N_{Re})_f}{(N_{Re})_{f'}} \cdot \frac{(C_p)_{f'}}{(C_p)_f}$$

Re-writing Equation 4.5

$$\frac{B}{B_o} = \left(\frac{(N_{Re})_f}{(N_{Re})_{f'}} \right)^{0.17} \left(\frac{K_{f'}}{K_f} \cdot \frac{\rho_{f'}}{\rho_f} \right)^{0.50} \left(\frac{(C_p)_{f'}}{(C_p)_f} \right)^{0.50} \quad \ldots \quad 4.6$$

From gas equation, at constant pressure,

$$\frac{\rho_{f'}}{\rho_f} = \frac{T_f}{T_{f'}} \quad \ldots\ldots \quad 4.7$$

and from International Critical Tables (26),

$$\frac{K_{f'}}{K_f} = \left(\frac{T_f + 125}{T_{f'} + 125}\right)\left(\frac{T_{f'}}{T_f}\right)^{\frac{3}{2}} \quad \ldots . \quad 4.8$$

Using Equations 4.7 and 4.8, Equations 4.4 and 4.6 can be re-written as :

$$\frac{A}{A_o} = \left(\frac{T_f + 125}{T_{f'} + 125}\right)\left(\frac{T_{f'}}{T_f}\right)^{\frac{3}{2}}\left(\frac{(N_{Pr})_{f'}}{(N_{Pr})_f}\right)^{0.20} \quad \ldots . \quad 4.9$$

$$\frac{B}{B_o} = \left(\frac{T_f + 125}{T_{f'} + 125}\right)^{\frac{1}{2}}\left(\frac{T_{f'}}{T_f}\right)^{\frac{1}{4}}\left(\frac{(N_{Pr})_f}{(N_{Pr})_{f'}}\right)^{0.17}\left(\frac{(C_p)_{f'}}{(C_p)_f}\right)^{0.50} . \quad 4.10$$

Variation of A and B with ambient air temperature can now be calculated.

Variation of Constants A and B.

Figure 18 shows the variation of the constants A and B , of Equation 4.1 with change in the ambient air temperature; these were plotted from Equations 4.9 and 4.10. The property values of air were taken from Eckert and Drake (27). The film temperature was used for selecting the properties with the hot-wire probe assumed to be at 450°F. It was found that the constant A increases slowly with the increase in ambient air temperature and B decreases. Increase in A is 4.2 per cent and the decrease in B is 1.2 per cent for 100°F change in ambient air temperature.

The change of A and B with ambient air temperature are both small and in opposite directions and therefore the expression ($A + B\sqrt{W}$) is essentially constant. Substituting a constant 'c' for ($A + B\sqrt{W}$), Equation 4.1 can be re-written for a constant velocity as

$$I^2 R_w = C (T_w - T_g)$$

Hence the power required by the probe varies linearly with the ambient air temperature. This justifies the shape of the curves obtained in Figure 16.

V. DESCRIPTION OF APPARATUS AND PROCEDURES

V. 1. FIN ASSEMBLIES

Few electric baseboard convectors consist of straight rectangular or annular fins but if the effect of the spacing or spacing to height ratio, can be determined for a simple geometry it will, at least, establish a guide for design. Thus an array of rectangular fins mounted on a calrod element as shown in Figure 8 was constructed.

The fins were assembled on the calrod heater element by silver soldering. This was achieved by assembling the fins with the proper spacing using a suitable fixture and then passing a heavy electric current through the base tube which melted the silver solder. Twelve thermocouples, six on each of two fins, were used to measure appropriate fin temperatures. One fin assembly is shown in Figure 8. Fin material was galvanised iron. The calrod diameter was 0.318 inches. The dimensions of the various fin assemblies tested were as given in Table 1.

TABLE 1

Set No.	H	W	S	t	S/H
1	1.905	1.905	0.4718	0.0282	0.248
2	1.905	1.905	0.3051	0.0282	0.160
3	1.905	1.905	0.2218	0.0282	0.116
4	1.905	1.905	0.1718	0.0282	0.090

Each set was tested with four different energy inputs from 180 watts to 440 watts.

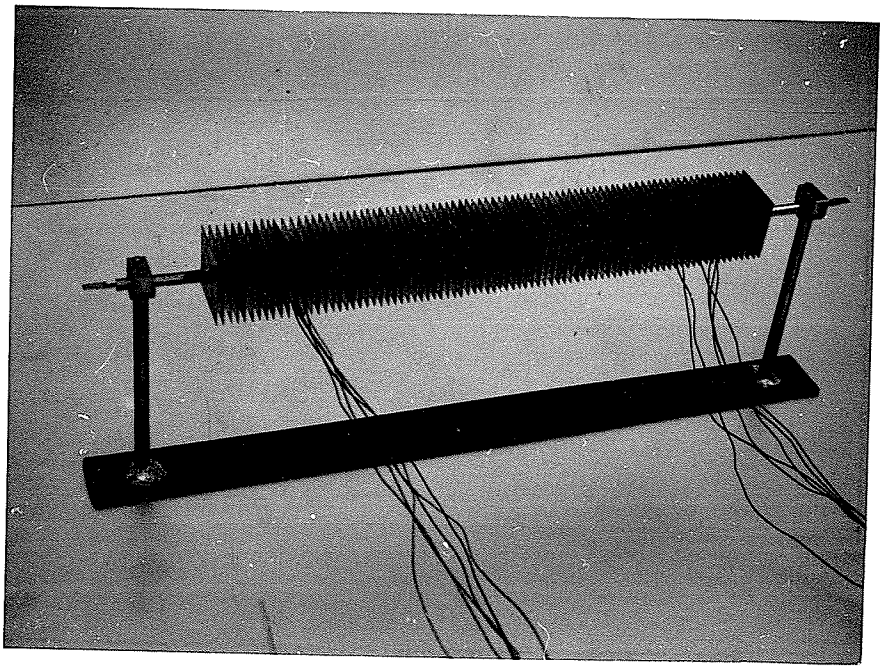

FIGURE 8. FIN ASSEMBLY

V. 2. TEMPERATURE MEASUREMENTS

Temperature traverse were made above each fin assembly for the four different power inputs. As indicated the heater was 18 inches long and readings were taken at 15 points equally spaced over the length of the heater. Typical plots are shown in Figures 19 to 22 inclusive. The traverses were made 7/8 inches above the fin assemblies and at the centre of the fin width. Average air temperatures were calculated from these results by graphical integration and are given in Figure 23.

The surface temperatures of the fins and the calrod were measured at the locations shown in Figure 26. A typical temperature distribution on the fin surface is shown in Figure 27.

Thermocouple were iron constantan of 30 gauge and 24 gauge for fin surface and probe temperature measurements respectively. A direct reading, manual balancing potentiometer was used to indicate the temperature and the accuracy was estimated to be $\pm$ 1^{o}F.

V. 3. POWER SUPPLY

The heater power source was 115 volts, Single Phase, AC, with a step down power transformer to regulate the supply for various desired power inputs. Power input was measured by an ammeter and a voltmeter. The voltmeter (0 - 150V) could be read to 2 per cent of full scale reading and the ammeter (0 - 10A) could be read to 1 per cent of the full scale reading. Thus the maximum error was estimated to be ± 10 watts.

The fin assemblies were tested over a power supply range of 180 watts to 440 watts.

V. 4. TRAVERSING MECHANISM

A traversing mechanism was designed and fabricated for traversing with the thermocouple and hot-wire probes over the fin assemblies. Figure 9 shows the picture of the traversing mechanism. As can be seen in the picture, it consists of a spiral which carries the support for the probes. The spiral also carried a scale to measure the displacement which could be read to ± 0.005 inches, but due to backlash the accuracy was estimated to be ± 0.025 inches.

As described in the section on temperature measurement the traverse involved readings at 15 points, equally spaced, across the outlet of the fin.

FIGURE 9. TRAVERSING MECHANISM

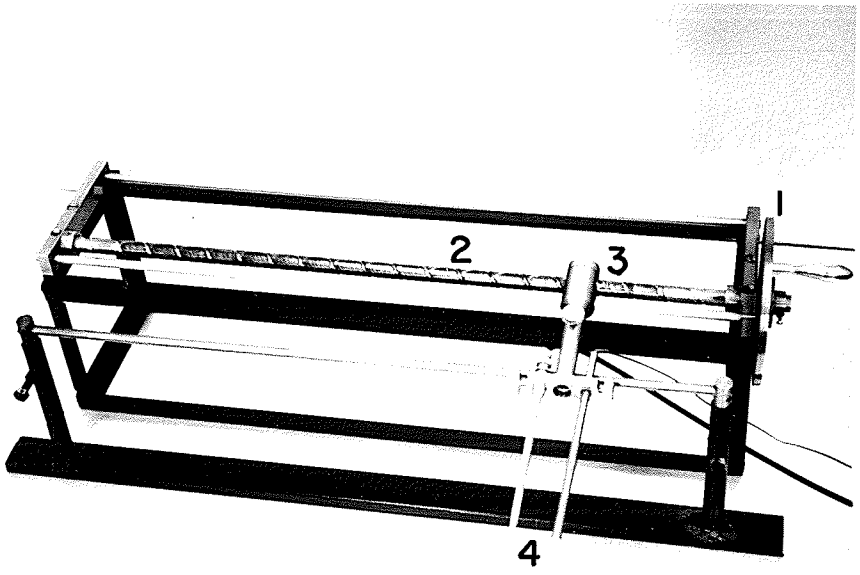

1. Disc Scale.
2. Spiral.
3. Probe Support.
4. Probes.

V. 5. INDUCED AIR FLOW MEASUREMENT

The amount of air induced over the fin assembly was measured by partly enclosing the fin element in an enclosure which allowed the induced air to come from one side of the enclosure as shown in Figure 10. The velocity of air being induced over the fin was estimated by measuring the velocity of the air at the entrance to the enclosure. The mass flow rate was then calculated from the velocity and the known area of the opening. The actual air flow leaving the heater would be greater than the estimated amount because of the air induced into the main stream above the heater. The values obtained therefore cannot be taken as the absolute values of the induced air flow over the fin, but they do represent a major part of it and are indicative of the relative induced air flow rates.

A Disa Constant Temperature Anemometer was used. Figure 11 shows the anemometer and the oscilloscope. Hot wire platinum plated tungsten probes, wire diameter 0.005 mm. and about 12 mm. long were used. The operating temperature of the probe was estimated to be 450°F as indicated in section IV.5.

The induced air flow rates were calculated for the various fin assemblies and for each power inputs to the heater element. As the variation in the velocity was small, average velocity as measured at the entrance was used to calculate the induced air flow rate. The results have been plotted in Figure 24.

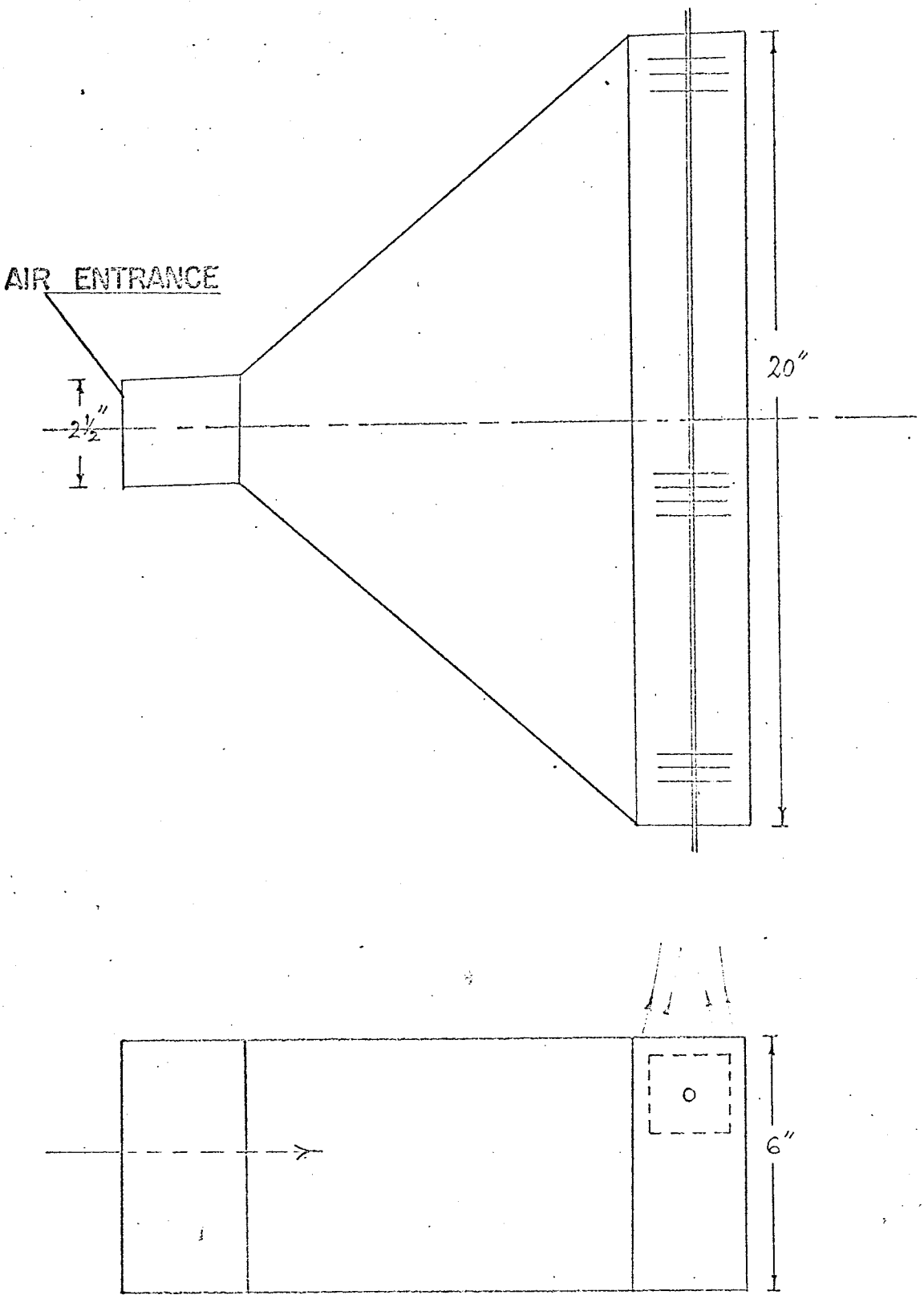

FIGURE 10. ENCLOSURE FOR INDUCED AIR FLOW MEASUREMENT

V. 6. VELOCITY MEASUREMENT OF DISCHARGED AIR

As already indicated, hot-wire anemometer was calibrated and used to measure the velocity of the discharged air from the fin element. To use the calibration curves of Figure 17, the air temperature at the point of measurement was required. A typical velocity traverse and the temperature at the corresponding points are given in Figure 25. The maximum error in measuring the low velocities was estimated to be ± 4 per cent.

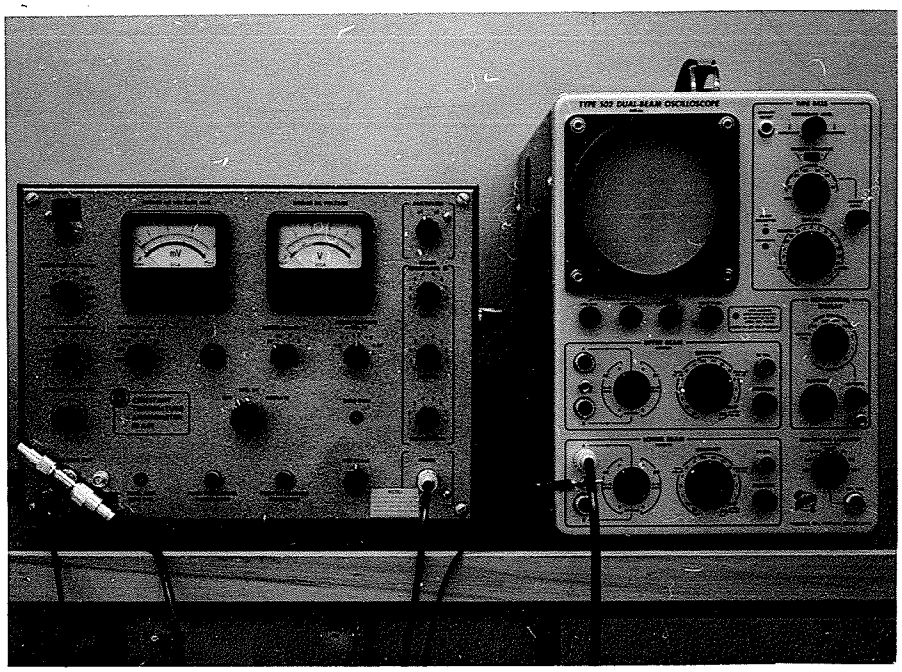

FIGURE 11. CONSTANT TEMPERATURE ANEMOMETER AND OSCILLOSCOPE

V. 7. SHADOWGRAPH TESTS

Various methods are used to visualize the details of fluid motion, and to enable such details to be photographed and analysed. The particular feature of the flow that is observed or recorded depends on the method of visualization and upon the experimental arrangement. Shadowgraph method was used to visualise the air flow pattern from the baseboard heaters because it provides a good indication of the flow from the heater and the experimental arrangement is simple.

Experimental Arrangement

A schematic diagram of the apparatus used for visualization of the air flow pattern above each of the heaters is shown in Figure 12. Plywood sheets were used to similate the wall and the floor. As shown in Figure 12, the shadowgraph cast on the tracing paper screen was photographed. This provides a record of an integrated average flow pattern over the length of the heater, which is commonly used as an indication of the flow over the heater. The light sources should be intense and well columinated; a condition which was not met by a projector. The camera was 35 millimetre with a f 1.8 lens and 300 ASA film. The results were not outstanding but they do create an impression of the quality of the flow pattern.

Figures 34 to 40 show the various enclosures tested. Photographs of the

air flow pattern obtained for the different types of enclosures studied are shown in Figures 41 to 46.

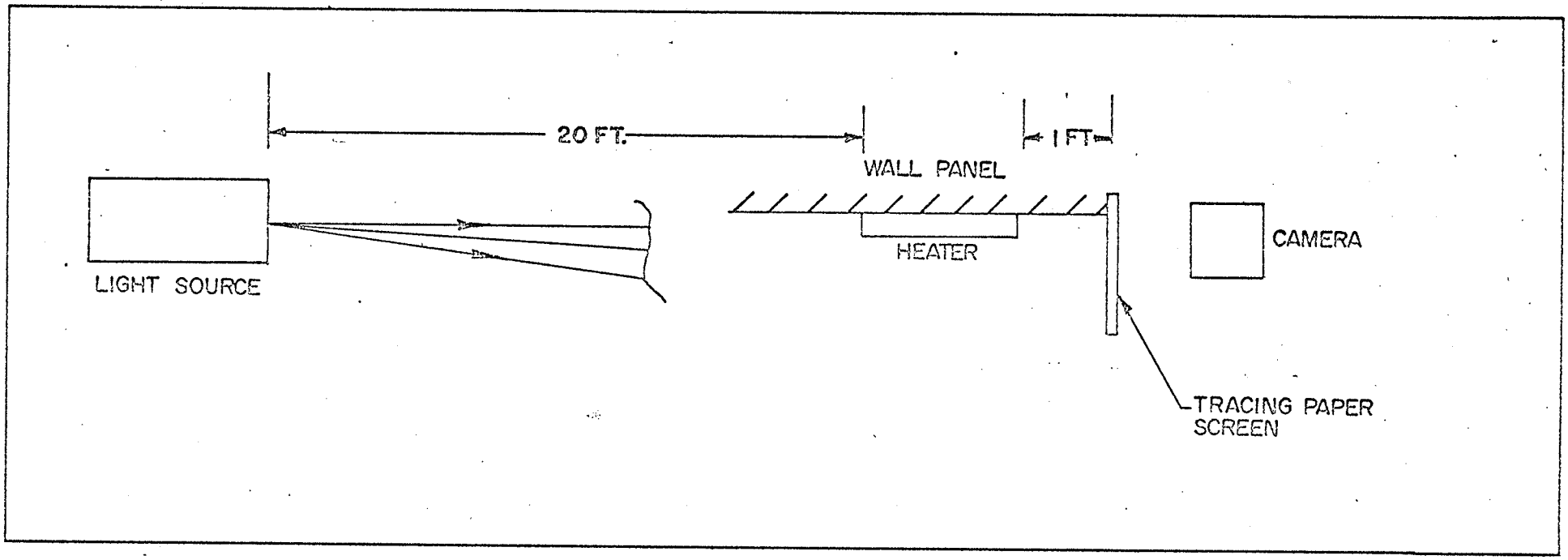

FIG. 12 SHADOWGRAPH SET-UP

To facilitate the flow-visualization of the heater enclosures, the side panels of the heaters were made of perspex. The side panels were 6 inches x 8 inches. Suitable holes were provided in these side panels to hold the heater element and to clamp any combination of front and back panels.

Shadowgraph Results.

A large number of front and back panel arrangements were tested. It was found that position and design of the back panel is not as important as the front panel in controlling the air flow from the heater. The quality of the photographs could be improved by using a more intense parallel light source. Higher ASA speed film would also help to improve the quality of the photographs.

Figure 41 is a photograph of a shadowgraph showing the air flow pattern from the heater when Enclosure No. 1 was used. This type of air flow, which is attracted by the wall, is typical of the available commercial electric baseboard heaters. A similar air flow pattern may be seen in Figure 43 when Enclosure No. 3 was used. The details of various enclosures are shown in Figures 33 to 39. Enclosure No. 1 was a simple rectangular shape enclosure. Enclosure No. 3 consisted on a back panel with the top oriented at an angle from the horizontal. The front panel was also angular. Enclosure No. 4 had the same back panel as No. 3, but front panel was different. The height of the front panel was slightly more than the back panel. Figure 44 shows the air flow pattern obtained

by using Enclosure No. 4. It can be seen that the air in this case has the tendency to be attracted towards the front panel. Shadowgraph studies were conducted with similar front panels of various heights and distances from the wall. It was found that the air flow was attracted and held by the vertical front panels as they were moved closer to the heater if the height was greater than the back panel. Such vertical front panels should be effective in decreasing wall streaking.

Enclosure No. 6 was a 'Z' shape enclosure. Figure 45 shows the air flow pattern from the heater when Enclosure No. 6 was used. It may be noticed that the front panel has helped the warm air to deflect away from the wall. Enclosure No. 7 proved to be an improvement over Enclosure No. 6 and Figure 46 shows the air flow pattern for No. 7. This enclosure helps in deflecting the air from the heater away from the wall so that intermixing of warm air with the room air may take place effectively; thus reducing the probability of wall streaking.

Based on these shadowgraphs, the probable mechanism by which the warm air is attracted by the wall is shown in Figures 13 and 14.

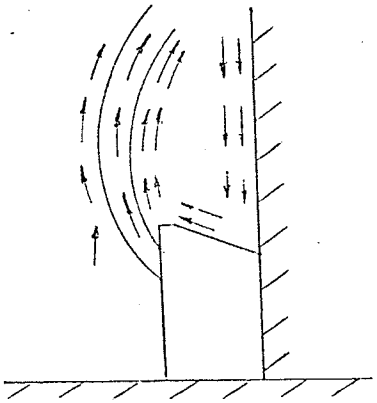

Figure 13. AIR FLOW PATTERN WITHOUT VERTICAL FRONT PANEL

Figure 13 shows what is considered to be a typical air flow pattern from a baseboard heater. The warm air from the heater moves upwards due to its low density and starts diffusing into the ambient air. The average velocity of this enlarged mass of warm air must decrease because of the fixed momentum. Had there been no wall or any other surface close to the flow, the diffusion of the warm air into ambient air would continue. The velocity of the warm air will decrease as the diffusion zone continues to grow. Without panels and wall the process of diffusion continues until the velocity is zero at some large distance from the heater. Due to the presence of the wall the velocity is increased at the wall, because of the reduction in diffusion and the pressure is lowered, which has the affect of inducing the flow toward the wall.

When a vertical front panel is placed in front of a heater, the low pressure exists on both sides of the main air flow. The deflection of the

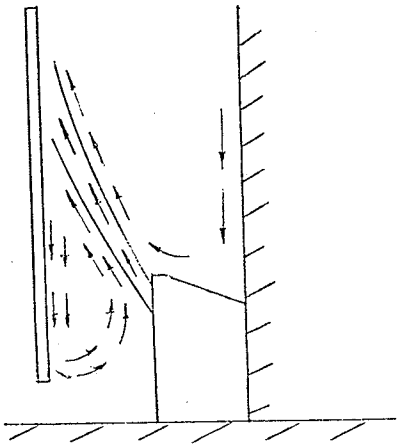

Figure 14. AIR FLOW PATTERN WITH VERTICAL FRONT PANEL

air now will depend upon the relative intensity of the reduced pressures. If the front panel is closer to the heater as compared to the distance

between the wall and the heater air outlet, the air will deflect towards the front panel as shown in Figure 14. Thus use of such front panel will help in reducing wall streaking. Any other stationery surface like drapes in front of the heater should also be helpful. Use of such arrangements will however depend upon other practical considerations.

VI. DISCUSSION OF RESULTS

The height to spacing ratio, H/S, is not an adequate parameter to analyse the results. This parameter has been used by Starner and McManus (16) and they found that the results could be explained satisfactorily as long as only the height was varied with a constant spacing. When the spacing and height both were varied, results could not be explained satisfactorily. The parameter H/S can therefore be used when spacing, S , is not varied and is used only to make the height, H , dimensionless. In the present investigation the height was kept constant and the spacing was varied. It was therefore felt that spacing should be used as the parameter in dimensionless form. Height was used to make the spacing dimensionless, giving the parameter S/H.

From the temperature distribution of the fin surface, Figure 27, it can be seen that the temperature at various points of the upper half of the surface are higher than at the corresponding points of the lower half of the surface. This will mean that value of local convection coefficients of the upper half of the surface are generally lower than at the corresponding points of the lower half of the surface. Performance of the fin could probably be improved by adding some higher convection coefficient surface and omitting some lower convection coefficient surface. It seems that it can be achieved if the calrod heater pass through a suitable position in the upper half of the fin rather than through the centre. To confirm this effect more experimentation will be required.

Figure 25 gives the velocity profile above one of the heaters. It can be noticed that velocity is generally higher at the point where the temperature is higher. Assuming that this behaviour is correct, some interesting conclusions can be drawn by studying the temperature traverses closely. It can be seen in Figure 19 that heater No. 1 (wide spacing) has quite a low temperature at the centre of its length. The temperature increases towards the ends and finally decreases as the ends of the heater approach. The similar characteristic is present in heater No. 2, though the variation of temperature is lower than in heater No. 1. In heaters No. 3 and No. 4 (small spacings), the temperature remains almost uniform along the length of the heater with small variations and the temperature decreases sharply near the ends of the heater. It can be concluded that at lower spacing to height ratios, the air flow from the heater is a single chimney flow but as the height to spacing ratio decreases the single chimney flow breaks into a multiple chimney flow.

Figure 23 shows the variation of average temperature difference between the discharged air and the ambient for the various fin arrays. It may be seen that for smaller spacing between the fins, the temperature difference is higher except for Set No. 2. In the case of Set No. 2, when power input is less than 260 watts, the average temperature difference is lower than that for Set No. 1 at the same power input. No explanation could be found for this irregularity.

The results of the fin efficiency calculations are given in Figure 28. Fins with spacing to height ratio of 0.16 have the highest fin efficiency.

Fins with spacing to height ration of 0.090 are more efficient than the fins with the ratio of 0.248. It can be noticed that no regular trend in the variation of the fin efficiency exists. The variation of the fin efficiency does not give any indication about the performance of the fin assembly as it is only effected by the conduction of heat through the fins. It does not take into consideration the convective heat transfer coefficient which is effected by changing the spacing between the fins.

Values of average convection coefficient and the heat transfer per degree temperature difference (Average Convection Conductance) were calculated as explained in Appendix B. The values of average convection coefficient for the fin surface for the various fin spacing are given in Figure 29. The average convection coefficient increases with an increase in the spacing to height ratio.

Figure 30 shows that an optimum value of average convection conductance exists. Figure 31 is a cross plot from Figure 30 and shows $\bar{h}A$ versus S/H for different base temperatures. The optimum value of S/H appears to be 0.12, but no information as to the effect of the base temperature on the optimum S/H is evident. It can however be seen that if the S/H ratio decreases below 0.11 the total heat transfer for the same base temperature will decrease even though additional heat transfer area were added to the fin assembly.

An attempt was made to use Fairbanks and Mark's (19) method to find out the optimum spacing between the fins and compare it with the results

obtained from this experimental investigation. To obtain the optimum spacing Fairbanks and Mark used fin efficiency which allowed for the fin temperature variation, by multiplying the temperature difference between the fin base and ambient air by the fin efficiency to get an average temperature difference. In the present case the average temperature of the fin was known from experimental results and so the process of multiplying the temperature difference of fin base and ambient air by the fin efficiency was eliminated.

For an average fin temperature of 250 F. the optimum spacing calculated from Fairbanks and Mark was 0.20 inches. The optimum spacing obtained from the present experiments is about 0.22 inches, which is 11 per cent higher than the value from Fairbanks and Mark. Recall that Fairbanks and Mark in addition to using the fin efficiency optimized the fin thickness by an iterative process based on Elenbaas's data. For small tube (calrod) diameters, the iterative process becomes ineffective because of small change of heat transfer caused by a change in the fin thickness. As may be seen from an example presented by them; the first approximation gave a spacing of 0.262 inches and after iteration they reached a value of 0.26 inches. The iterative procedure seems to be useful only if the diameter of the tube is large as compared to the fin dimensions. Then there is some substantial variation in heat transfer with fin thickness. If the tube diameter is small as compared to the fin dimensions, then the thickness of the fin should be selected for considerations other than the heat transfer effectiveness.

Figure 32 shows a family of curves for each S/H plotted against dimensionless parameter $N_{Gz}/\Delta T.\beta$ and heat input. Figure 33 is a cross plot of Figure 32 showing variation of $N_{Gz}/\Delta T.\beta$ versus S/H. The parameter $N_{Gz}/\Delta T.\beta$ was chosen to indicate the effectiveness of the fin array in producing an induced velocity with a fixed convection potential ($\Delta T.\beta$) and has been referred to as Induced Flow Parameter. Figure 32 shows that wider spacing between the fins is better suited to the higher heat inputs. This can be contributed to the small increase in average temperature difference between the discharged air and the ambient as compared to a rapid increase in induced air flow rate. Figure 33 shows that a maximum value of the Induced Flow Parameter does occur at S/H of 0.16 and heat inputs of up to 200 watts/ft. From this it can be concluded that the S/H should not be less than 0.16. Also recall that the maximum heat transfer occured at S/H of 0.12.

For high heat inputs (Above 200 watts/ft.) the Induced Flow Parameter does not reach a maximum. The limit is the maximum temperature of the fin as dictated by the code for reason of safety. A study of Figures 31 and 33 indicate that S/H should not be less than 0.18 for good flow conditions but the heat transfer effectiveness has decreased from the maximum heat transfer conditions. The temperature of the fin surface will commence to rise if spacing is increased any further.

VII CONCLUSIONS

1. For a hot-wire probe, in case of constant temperature anemometer it was found by experiments that the variation of power required by the probe varied linearly with the temperature of the ambient fluid, flowing at a constant velocity. A theoretical analysis verified the reason for the linearity.
2. The average convection coefficient over the fins decreases as the spacing to height ratio decreases. For fins of 1.9 inches height, the heat transfer per unit temperature difference has a maximum value at the spacing to height ratio of about 0.12 above and below which the heat transfer decreases. Addition of extra heat transfer surface at this stage will decrease the total heat transfer.
3. It was found that the spacing to height ratio of about 0.18 is most suitable for the fin element. Though the heat transfer effectiveness has decreased from the maximum heat transfer value; this value of spacing to height ratio is based on good flow conditions.
4. It was found that proper front panel design is very important for deflecting the discharged air from the heater away from the wall. The back panel is not as important as the front panel.
5. It was found that a vertical front panel as shown in Figure 37 is very effective in deflecting the discharged air from the heater away from the wall. The enclosure shown in Figure 40 was also found to be quite effective in deflecting the discharged air away from the wall.

BIBLIOGRAPHY

(1) Schmidt, E., and Beckmann, W., Techn. Mech. u. Thermodynamik. Vol. 1, No. 10, pp 341 - 349; cont'd Vol. 1, No. 11, pp 391 - 406.

(2) Eckert, E.R.G., and Jackson, T.W., "Analysis of Turbulent Free Convection Boundary Layer on Flat Plate", NACA Report 1015, July, 1950.

(3) Eckert, E.R.G., and Soehnghen, E., "Interferometeric Studies on the Stability and Transition to Turbulence of Free Convection Boundary Layer", Proc. of the General Discussion on Heat Transfer (ASME-IME, 1951), pp 321 - 323.

(4) McAdams, W.H., "Heat Transmission", McGraw Hill Book Company Inc., 1954, pp 167 - 175.

(5) Carpenter, L.G., and Wassel, H.C., "The Loss of Heat by Natural Convection from Parallel Vertical Plates in Air", The IME Proceedings, Vol. 128, 1934, pp 439 - 458.

(6) Elenbaas, W., "Heat Dissipation of Parallel Plates by Free Convection", Physica IX, No. 1, 1942, pp 1 - 28.

(7) Elenbaas, W., "Dissipation of Heat by Free Convection", Part II, Phillips Res. Rep.: Part I, Vol. 3, pp 338 - 360; Part II, Vol. 3, pp 450 - 465, 1948.

(8) Ostrach, S., "Laminar Natural Convection and Heat Transfer of Fluids With and Without Heat Sources in Channels With Constant Wall Temperatures", NACA Technical Note 2863, 1952.

(9) Bodoia, J.R., and Osterle, J.F., "The Development of Free Convection Between Heated Vertical Plates", Trans. ASME, Series C, Vol. 84, 1962, pp 40 - 43.

(10) Siegel, R., and Norris, R.H., "Tests of Free Convection in a Partially Enclosed Space between Two Heated Vertical Plates", Trans. ASME, Vol. 79, 1957, pp 663 - 672.

(11) Murray, W.M., "Heat Dissipation Through an Annular Disc or Fin of Uniform Thickness", Trans. ASME, Vol. 60, 1938, pp A.78 - A.80.

(12) Gardner, K.A., "Efficiency of Extended Surfaces", Trans. ASME, Vol. 67, 1945, pp 621 - 631.

(13) Weiner, J.H., Gross, D., and Paschikis, V., "An Experimental Determination of Local Boundary Conductances for an Unbaffled Circular Finned Cylinder", AME - ASME Heat Transfer Discussion, 1951, pp 154 - 159.

(14) Edwards, J.A. and Chaddock, J.B., "Free Convection and Radiation Heat Transfer from Fin On Tube Heat Exchanges", ASME Paper No. 62-WA-205, 1962.

(15) Knudsen, J.G., and Pan, R.B., "Natural Convection Heat Transfer from Transverse Finned Tubes", Sixth National Heat Transfer

Conference, Preprint No. 19, 1963.

(16) Starner, K.E., and McManus, Jr., H.N., "An Experimental Investigation of Free Convection Heat Transfer from Rectangular Fin Arrays", Trans. ASME, Series C, Vol. 85, 1963, pp 273 - 278.

(17) Welling, J.R., and Wooldridge, C.B., "Free Convection Heat Transfer Coefficients From Rectangular Vertical Fins", Trans. ASME, Series C, Vol. 87, Nov., 1965, pp 439 - 444.

(18) Harahap, F., and McManus, Jr. H.N., "Natural Convection Heat Transfer from Horizontal Rectangular Fin Arrays", Trans. ASME, Series C, Vol. 89, Feb. 1967, pp 32 - 38.

(19) Fairbanks, D.R., and Mark, M., "An Optimization Procedure for Finning in Free Convection", ASME Paper No. 65-HT-12, 1965.

(20) Goldsmith, A., Final Report IITRI Project No. N8009 "Experimental Rating of Baseboard Type Electric Heaters with Regard to Soiling Characteristics", IIT Research Institute, Technology Centre, Chicago, U.S.A.

(21) Gieseke, J.A., Final Report on "Causes and Reduction of Wall Discolouration from Baseboard Heaters", Battelle Memorial Institute, Columbus Laboratories, Columbus, U.S.A., 1966.

(22) Baljet, A.F., "Functional Design of Baseboard Type Electric Heaters", Research Quarterly, Ontario Hydro, Vol. 18, No. 1, First Quarter, 1966, pp 10 - 13.

(23) Goldstein, S., "Modern Developments in Fluid Dynamics", Vol. II, Dover Publications Inc., 1965, pp 638 - 643.

(24) Langhaar, H.L., "Dimensional Analysis and Theory of Models", John Wiley and Sons, 1965, pp 29 - 43.

(25) Hinze, J.O., "Turbulence", McGraw Hill Book Company, Inc., 1959, pp 75 - 119.

(26) Anon, "International Critical Tables", Vol. V. McGraw Hill Book Company, Inc., 1929, p 10.

(27) Eckert, E.R.G., and Drake, R.M., "Heat and Mass Transfer", McGraw Hill Book Company, Inc., 1954, p 504.

(28) Almquist, P., and Legath, E., "The Hot-Wire Anemometer at Low Air Velocities", DISA Information, published by DISA, Herlev, Denmark.

APPENDIX A

DIMENSIONAL ANALYSIS

A dimensional analysis of the variables involved was carried out. The following variables were considered -

Variables	Symbol	Dimensions
Induced air flow rate	q_v	L^3T^{-1}
Temperature difference between the air leaving the heater and room temperature	ΔT	θ
Temperature potential causing the induced air flow	ΔT_p	θ
Density of air	ρ	ML^{-3}
Velocity of air	v	LT^{-1}
Heat flow rate	Q	$ML^{-2}T^{-3}$
Absolute viscosity of air	μ	$ML^{-1}T^{-1}$
Spacing between the fins	S	L
Height of the fin	H	L
Acceleration due to gravity	g	LT^{-2}
Specific heat of air	C_p	$L^2T^{-2}\theta^{-1}$
Coefficient of expansion	β	Θ^{-1}
Thermal conductivity of air	K	$MLT^{-3}\theta^{-1}$

Two dimensionless groups can be obtained by inspection :

$$\frac{H}{S} \quad \text{and} \quad \frac{\Delta T}{\Delta T_p}$$

$$F\left(q_v, \Delta T, \rho, \upsilon, Q, \mu, H, g, c_p, \beta, K\right) = \text{CONSTANT } C$$

Following the procedure from Langhaar (24), the dimensional matrix is

	1	2	3	4	5	6	7	8	9	10	11
	q_v	ΔT	ρ	υ	Q	μ	H	g	c_p	β	K
M	0	0	1	0	1	1	0	0	0	0	1
L	3	0	-3	1	-2	-1	1	1	2	0	1
T	-1	0	0	-1	-3	-1	0	-2	-2	0	-3
θ	0	1	0	0	0	0	0	0	-1	-1	-1

The homogenous linear algebraic equations can be written as:

$$K_3 + K_5 + K_6 + K_{11} = 0$$

$$3K_1 - 3K_3 + K_4 + 2K_5 - K_6 + K_7 + K_8 + 2K_9 + K_{11} = 0$$

$$-K_1 - K_4 - 3K_5 - K_6 - 2K_8 - 2K_9 - 3K_{11} = 0$$

$$K_2 - K_9 - K_{10} - K_{11} = 0$$

Solving these equations for K_8, K_9, K_{10}, K_{11}, we have:

$$K_8 = 2K_1 - K_3 + K_5 + K_7$$

$$K_9 = -\frac{5}{2}K_1 + \frac{5}{2}K_3 - \frac{1}{2}K_4 - K_5 + K_6 - K_7$$

$$K_{10} = \frac{5}{2}K_1 + K_2 - \frac{3}{2}K_3 + \frac{1}{2}K_4 + 2K_5 + K_7$$

$$K_{11} = -K_3 - K_5 - K_6$$

Now the matrix of solution can be written as:

	q_v	ΔT	ρ	v	Q	μ	H	g	c_p	β	k
	K_1	K_2	K_3	K_4	K_5	K_6	K_7	K_8	K_9	K_{10}	K_{11}
π_1	1	0	0	0	0	0	0	2	$-\frac{5}{2}$	$\frac{5}{2}$	0
π_2	0	1	0	0	0	0	0	0	0	1	0
π_3	0	0	1	0	0	0	0	-1	$\frac{5}{2}$	$-\frac{3}{2}$	-1
π_4	0	0	0	1	0	0	0	0	$-\frac{1}{2}$	$\frac{1}{2}$	-1
π_5	0	0	0	0	1	0	0	1	-1	2	-1
π_6	0	0	0	0	0	1	0	0	+1	0	-1
π_7	0	0	0	0	0	0	1	1	-1	-1	0

So the complete set of dimensionless products is:

$$\pi_1 = q_v g^2 \left(\frac{\beta}{c_p}\right)^{5/2}$$

$$\pi_2 = \Delta T . \beta$$

$$\pi_3 = \frac{\rho C_p^2}{g K \beta} \sqrt{\frac{C_p}{\beta}}$$

$$\pi_4 = v \sqrt{\frac{\beta}{C_p}}$$

$$\pi_5 = \frac{Q g \beta^2}{C_p K}$$

$$\pi_6 = \frac{\mu C_p}{K} = N_{Pr}$$

$$\pi_7 = \frac{H g \beta}{C_p}$$

$$\pi_8 = \frac{H}{S}$$

$$\pi_9 = \frac{\Delta T}{\Delta T_p}$$

These dimensionless groups can now be reorganised as follows:

$$\frac{\pi_5}{\pi_7 . \pi_2} = \frac{Q}{H . \Delta T . K} = \frac{\bar{h} . D}{K} = N_{Nu}$$

(D being any length parameter.)

$$\frac{\pi_1 \pi_3}{\pi_7} = \frac{q_v . \rho . C_p}{K . H} = N_{Gz}$$

$$\frac{\pi_2 \cdot \pi_3^2 \pi_7^3}{\pi_6^2} = \frac{H^3 \rho^2 g}{\mu^2} (\beta \cdot \Delta T) = N_{Gr}$$

$$\frac{\pi_5 \cdot \pi_7^{-2}}{\pi_2 \cdot \pi_3 \cdot \pi_4} = \frac{Q}{H^2 \Delta T} \cdot \frac{1}{c_p v \rho} = \frac{\bar{h}}{c_p v \rho} = N_{St}$$

The transformed dimensionless groups can now be written as

$$N_{Nu} = A (N_{Gr})^m (N_{Gr})^n (N_{St})^p (N_{Pr})^q (\Delta T \cdot \beta)^r \left(\frac{H g \beta}{c_p}\right)^x \left(\frac{H}{S}\right)^y \left(\frac{\Delta T}{\Delta T_p}\right)^z$$

APPENDIX B

CALCULATION OF AVERAGE CONVECTION COEFFICIENT

Average convection coefficient for the fin was calculated from the energy input to the calrod heater on the basis of following assumptions :

(1) Convection coefficient is constant all over the fin surface and is equal to the average convection coefficient.

(2) Convection coefficient over the fin tip surface and calrod heater surface is same as on the fin surface.

(3) The temperature of the fin was uniform and equal to the average temperature as calculated below.

The average fin temperature was calculated by drawing isotherms of the fin surface. A typical set of isotherms is shown in Figure B-1. Considering two isotherms T_1 and T_2, let the area enclosed between these isotherms be A_r. Now assuming that the temperature of the area surrounded by the isotherms can be assumed to be uniform Temperature T_r, which is given by

$$T_r = \frac{T_1 + T_2}{2}$$

So the average fin temperature is now given by

$$\bar{T} = \frac{\Sigma A_r T_r}{\Sigma A_r}$$

Convection conductance and the average convection coefficient can now be calculated as follows

$$\bar{h} A = \frac{Q}{(\bar{T} - T_g)}$$

and,

$$\bar{h} = \frac{Q}{A(\bar{T} - T_g)}$$

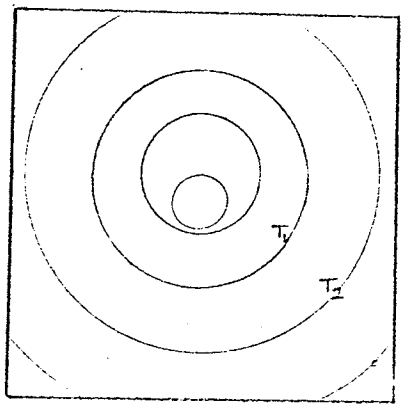

Figure B-1. TEMPERATURE VARIATION ON FIN SURFACE

APPENDIX C

CALCULATION OF FIN EFFICIENCY

Fin efficiency is defined as the ratio of the heat transferred by the fin, to the heat which would have been transferred by the same fin had it been at a uniform temperature equal to the base temperature, that is, fin of infinite thermal conductivity.

So,

$$\eta = \frac{Q}{Q_o}$$

$$= \frac{\bar{h} A (\bar{T} - T_g)}{\bar{h} A (T_o - T_g)}$$

$$= \frac{\bar{T} - T_g}{T_o - T_g}$$

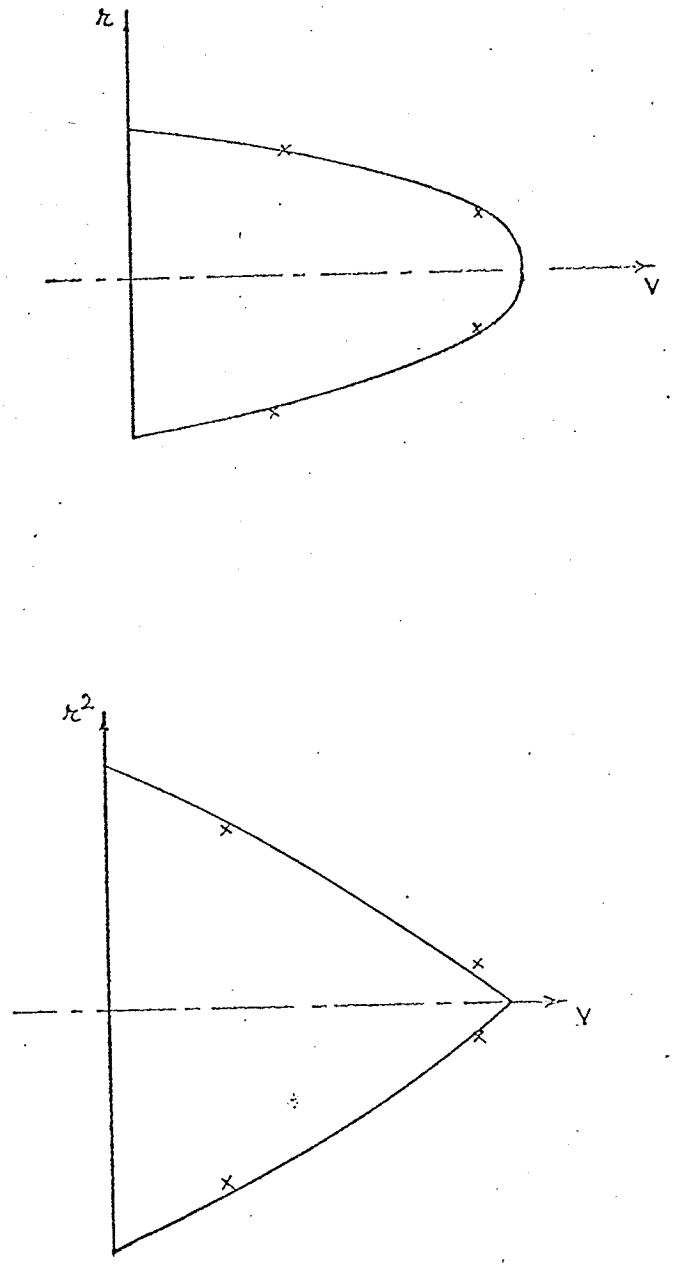

FIG. 15 VELOCITY PROFILE ACROSS THE TUBE

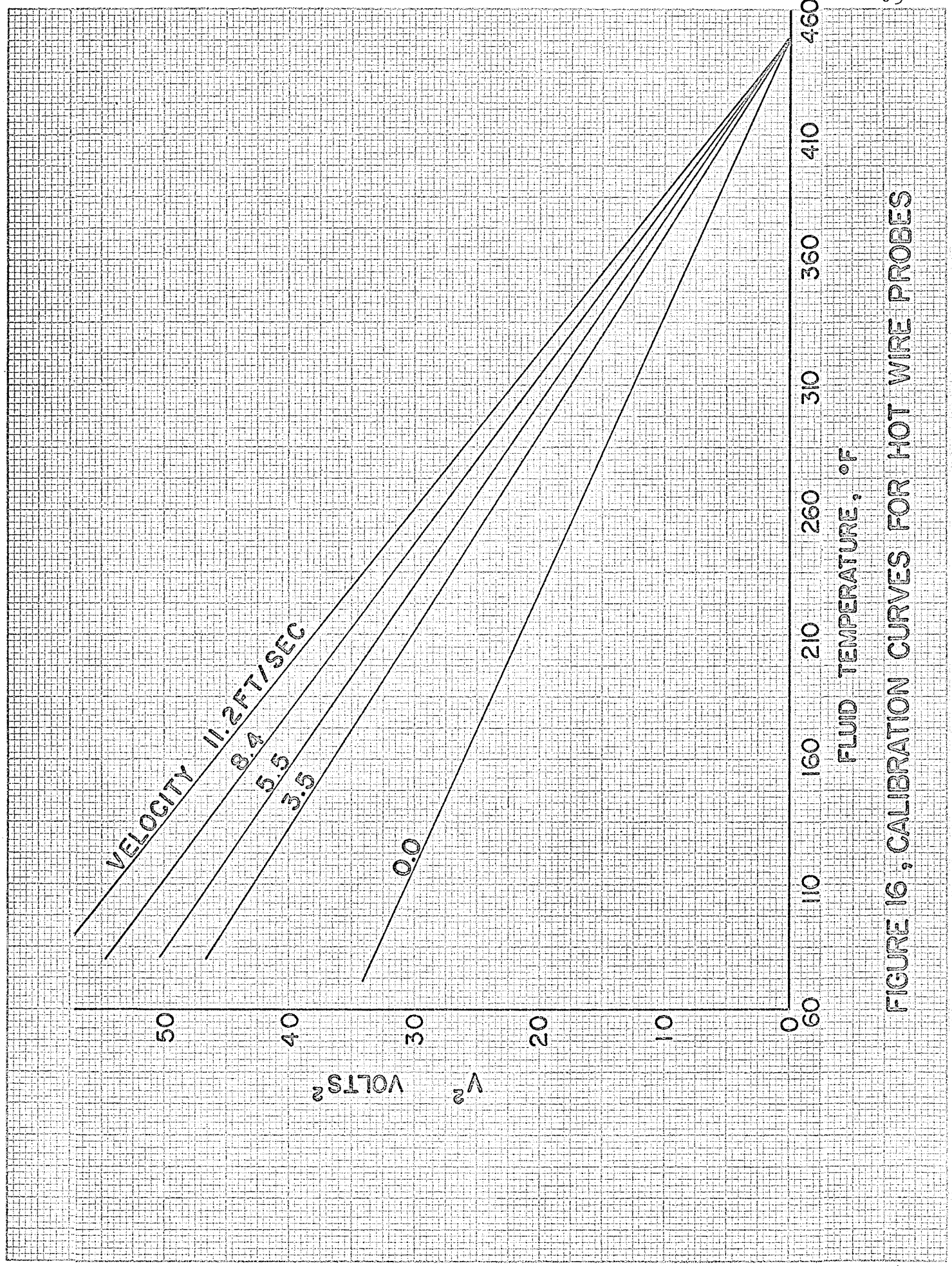

FIGURE 16 - CALIBRATION CURVES FOR HOT WIRE PROBES

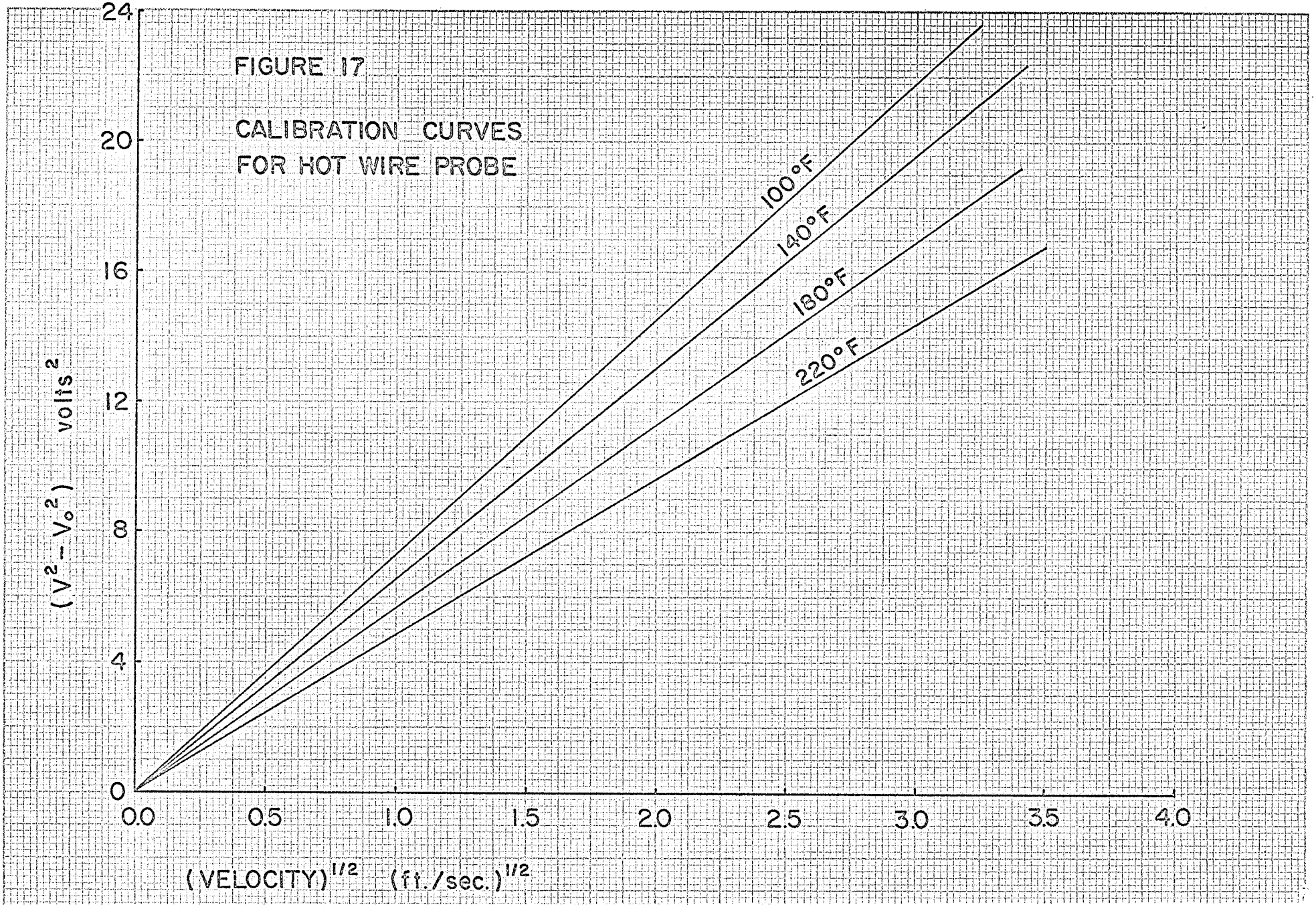
FIGURE 17
CALIBRATION CURVES
FOR HOT WIRE PROBE
100°F
140°F
180°F
220°F
24
20
16
12
8
4
0
$(V^2-V_o^2)$ volts^2
0.0
0.5
1.0
1.5
2.0
2.5
3.0
3.5
4.0
(VELOCITY)$^{1/2}$ (ft./sec.)$^{1/2}$

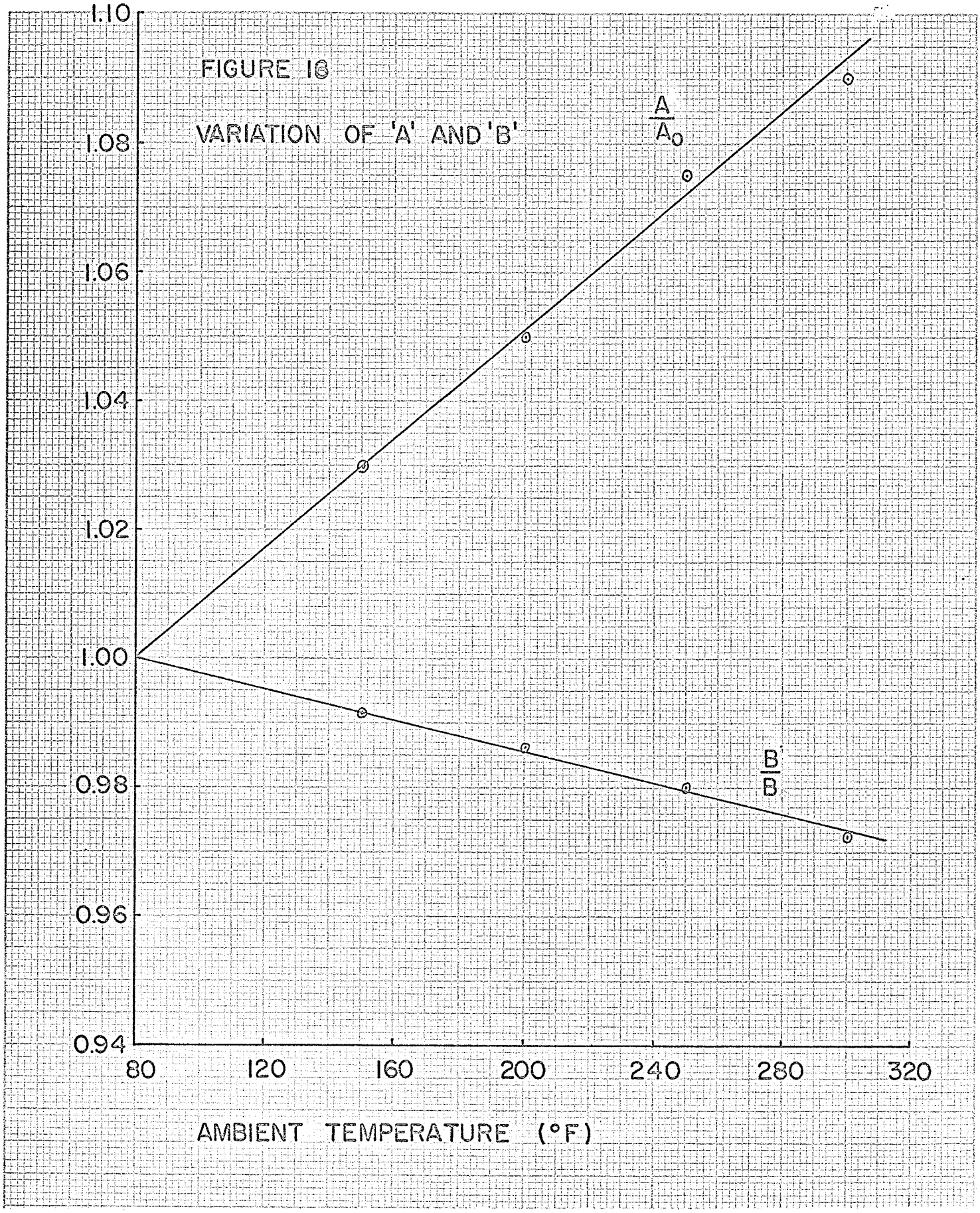
FIGURE 16
VARIATION OF 'A' AND 'B'
A/A0
B/B
1.10
1.08
1.06
1.04
1.02
1.00
0.98
0.96
0.94
80
120
160
200
240
280
320
AMBIENT TEMPERATURE (°F)

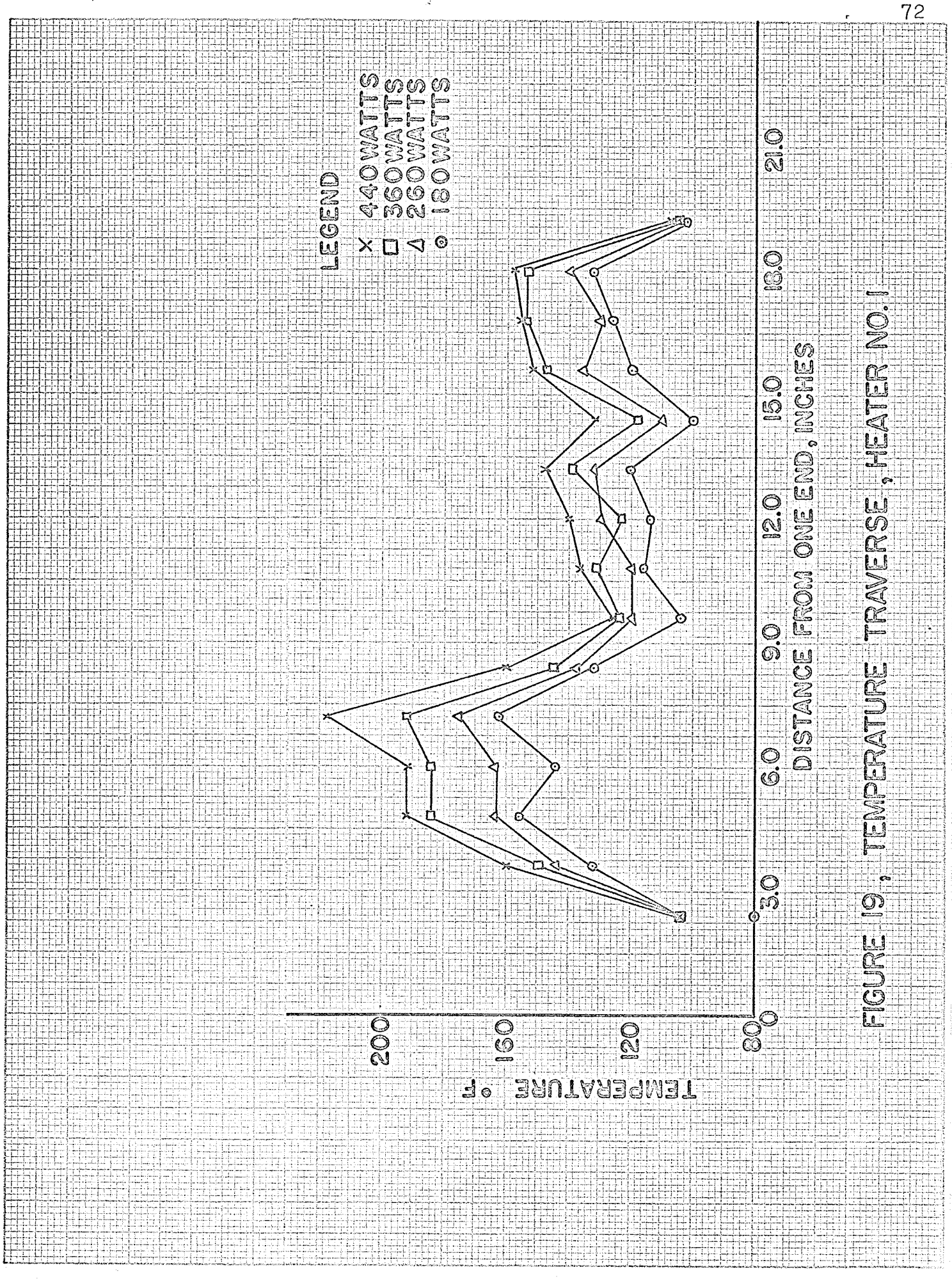

FIGURE 19 ; TEMPERATURE TRAVERSE, HEATER NO. 1

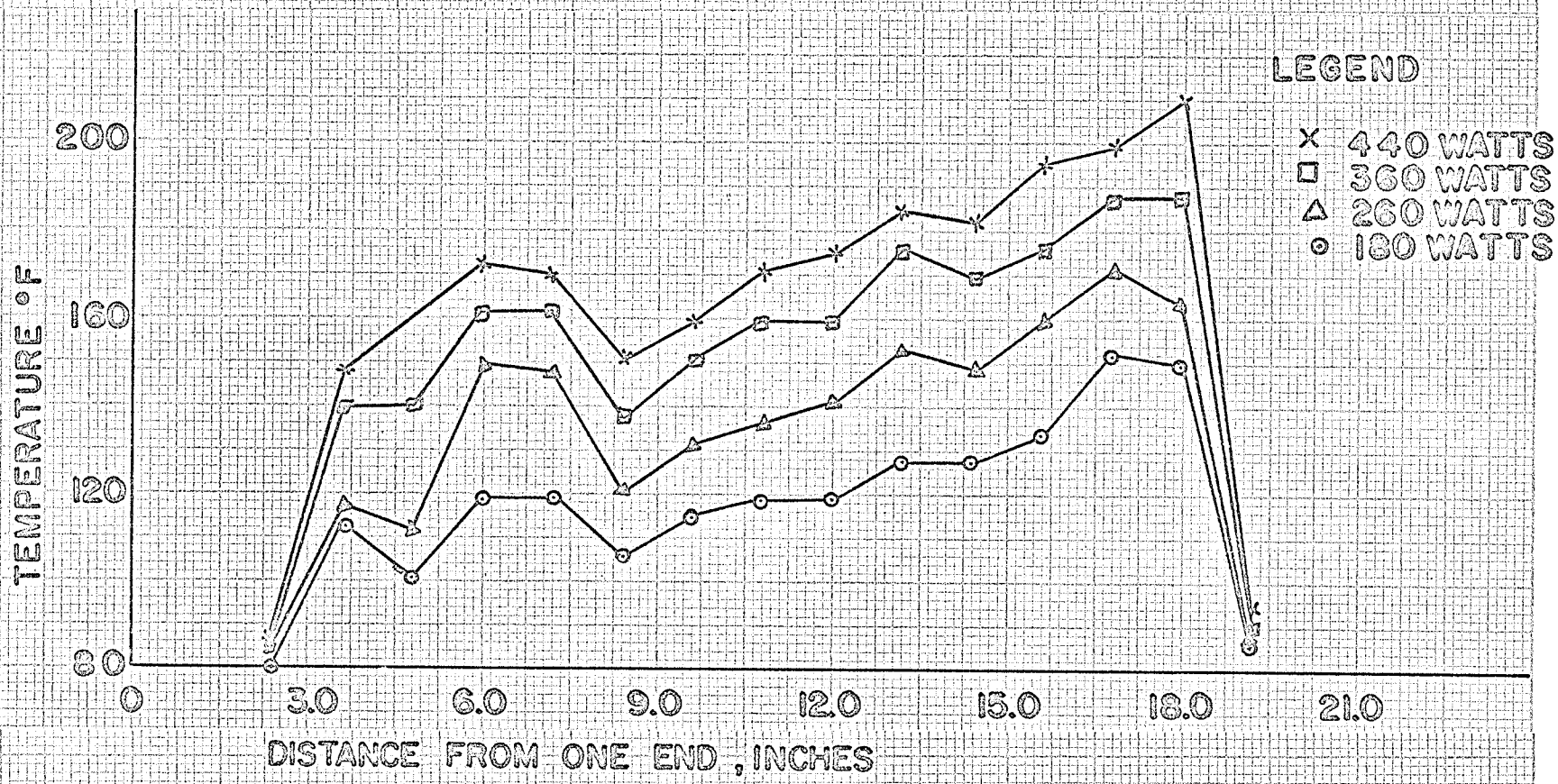

FIGURE 20, TEMPERATURE TRAVERSE, HEATER NO. 2

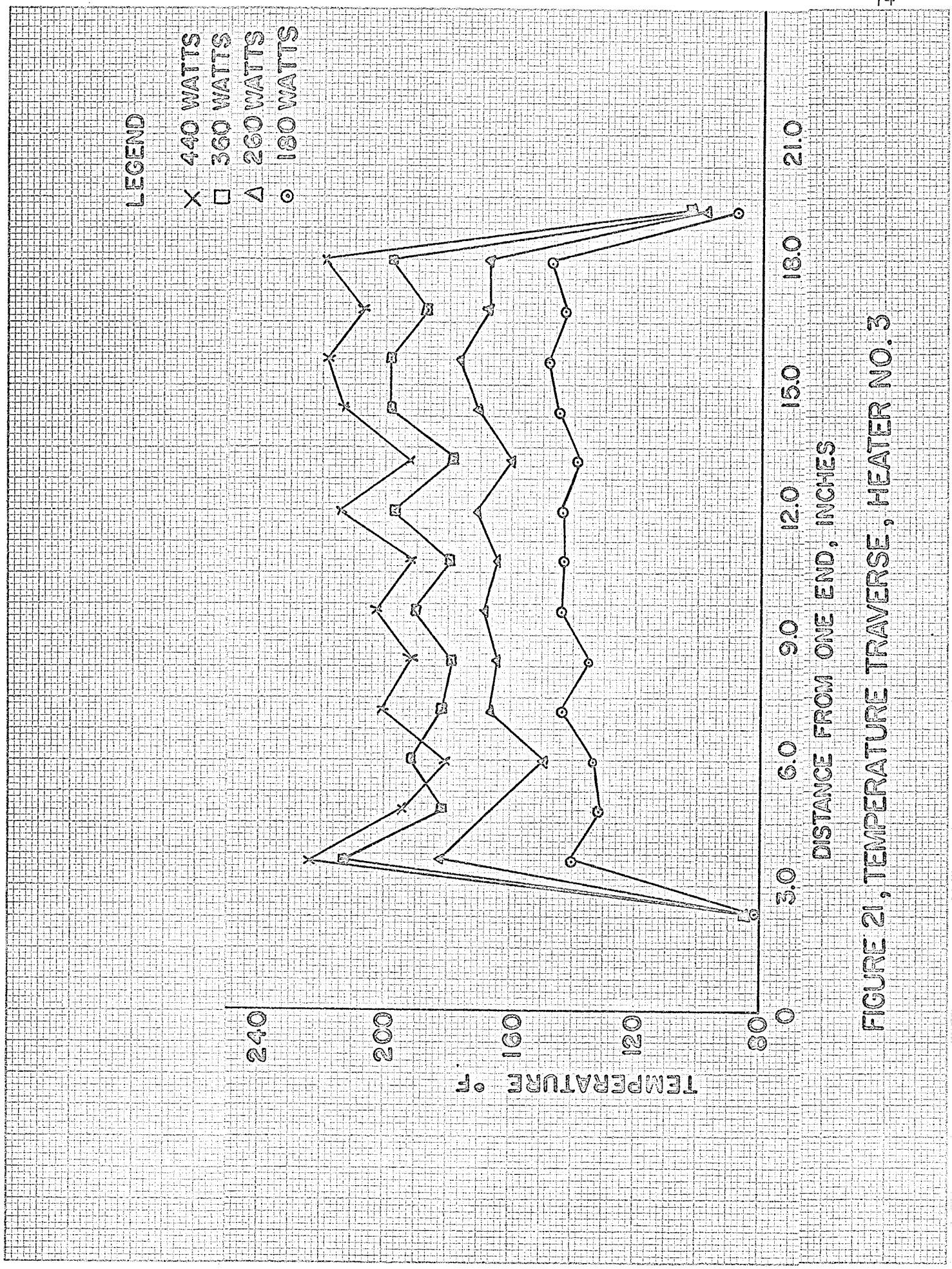

FIGURE 21, TEMPERATURE TRAVERSE, HEATER NO. 3

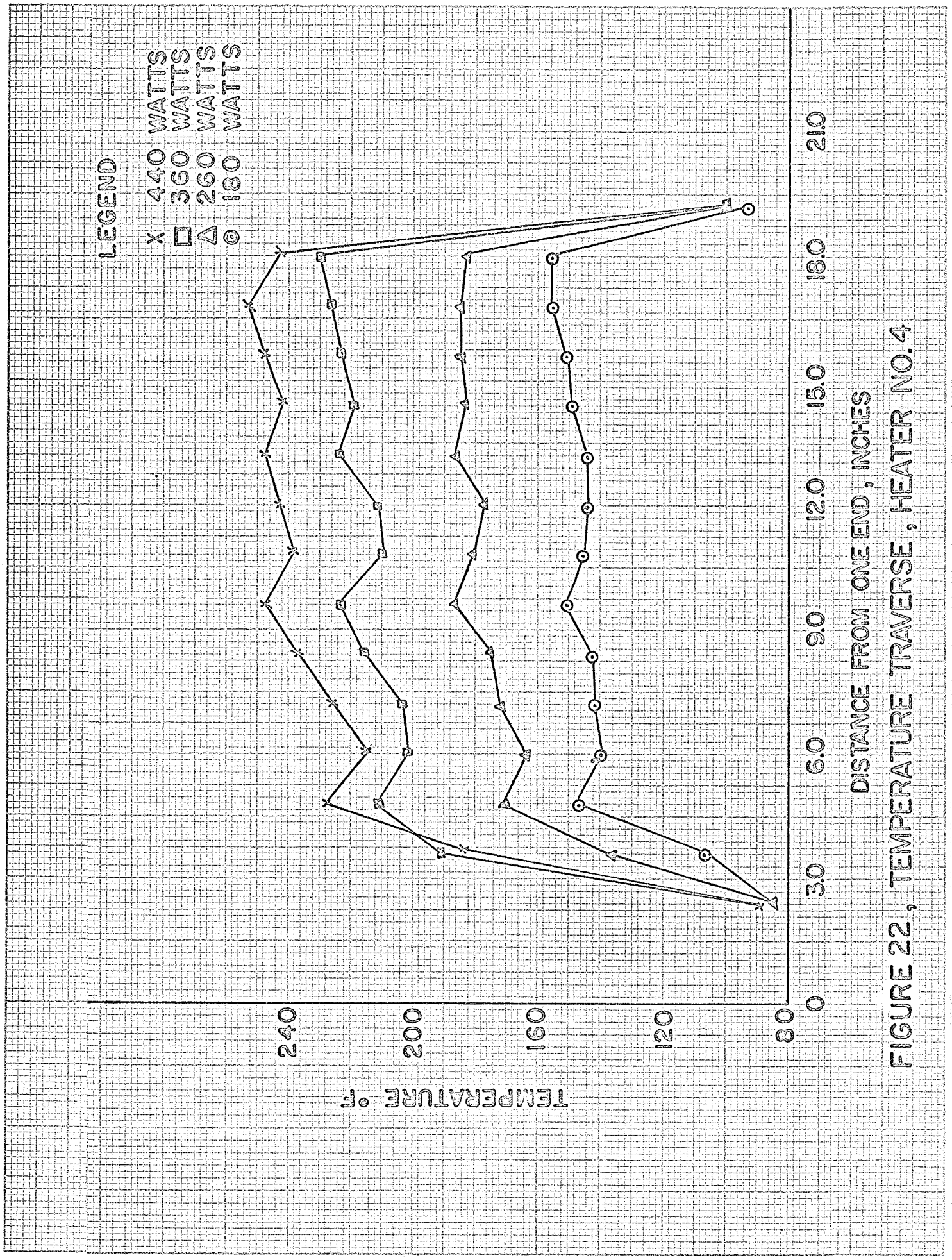

FIGURE 22, TEMPERATURE TRAVERSE, HEATER NO. 4

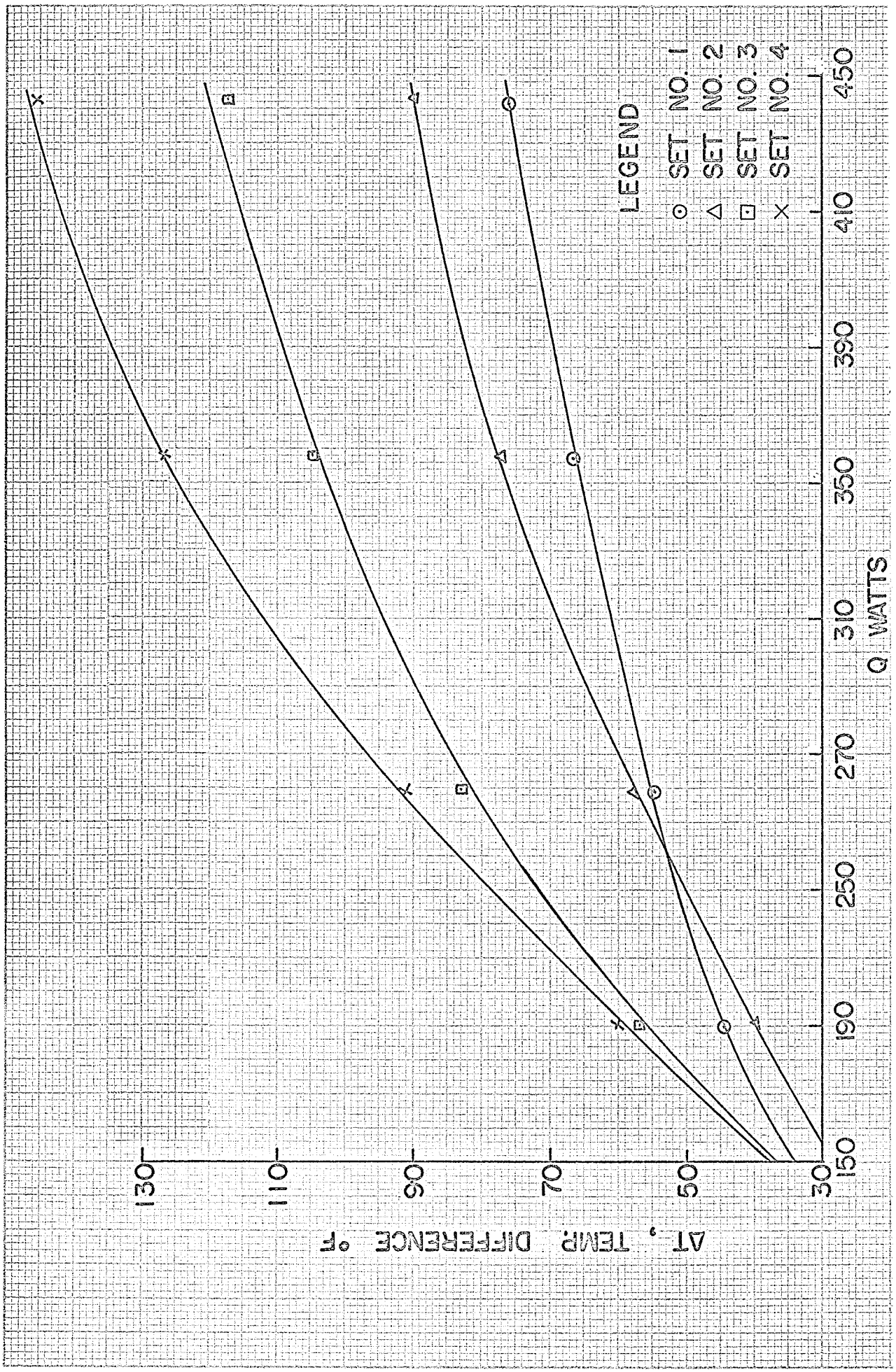

FIGURE 23, VARIATION OF AVERAGE TEMPERATURE DIFFERENCE

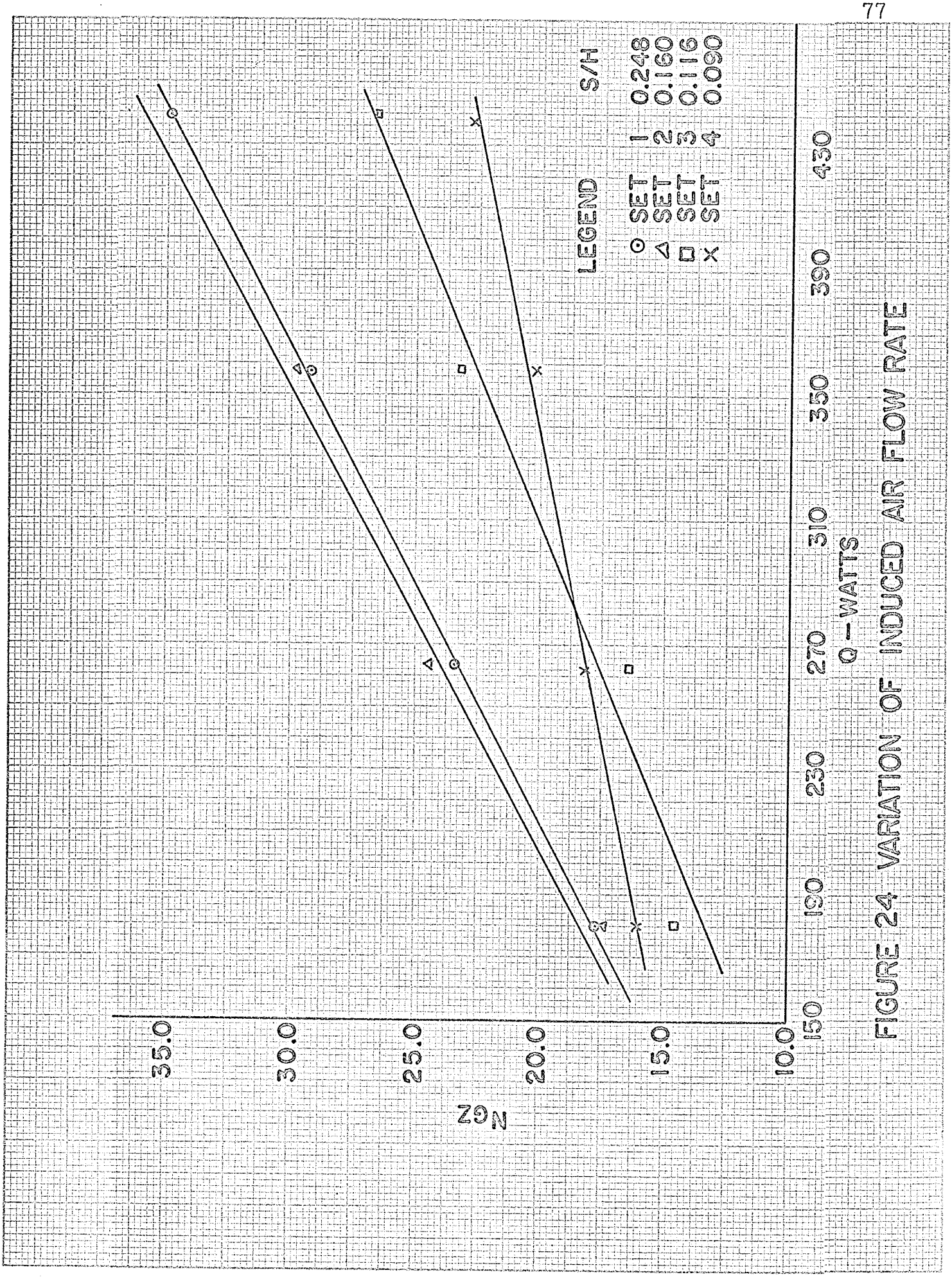

FIGURE 24. VARIATION OF INDUCED AIR FLOW RATE

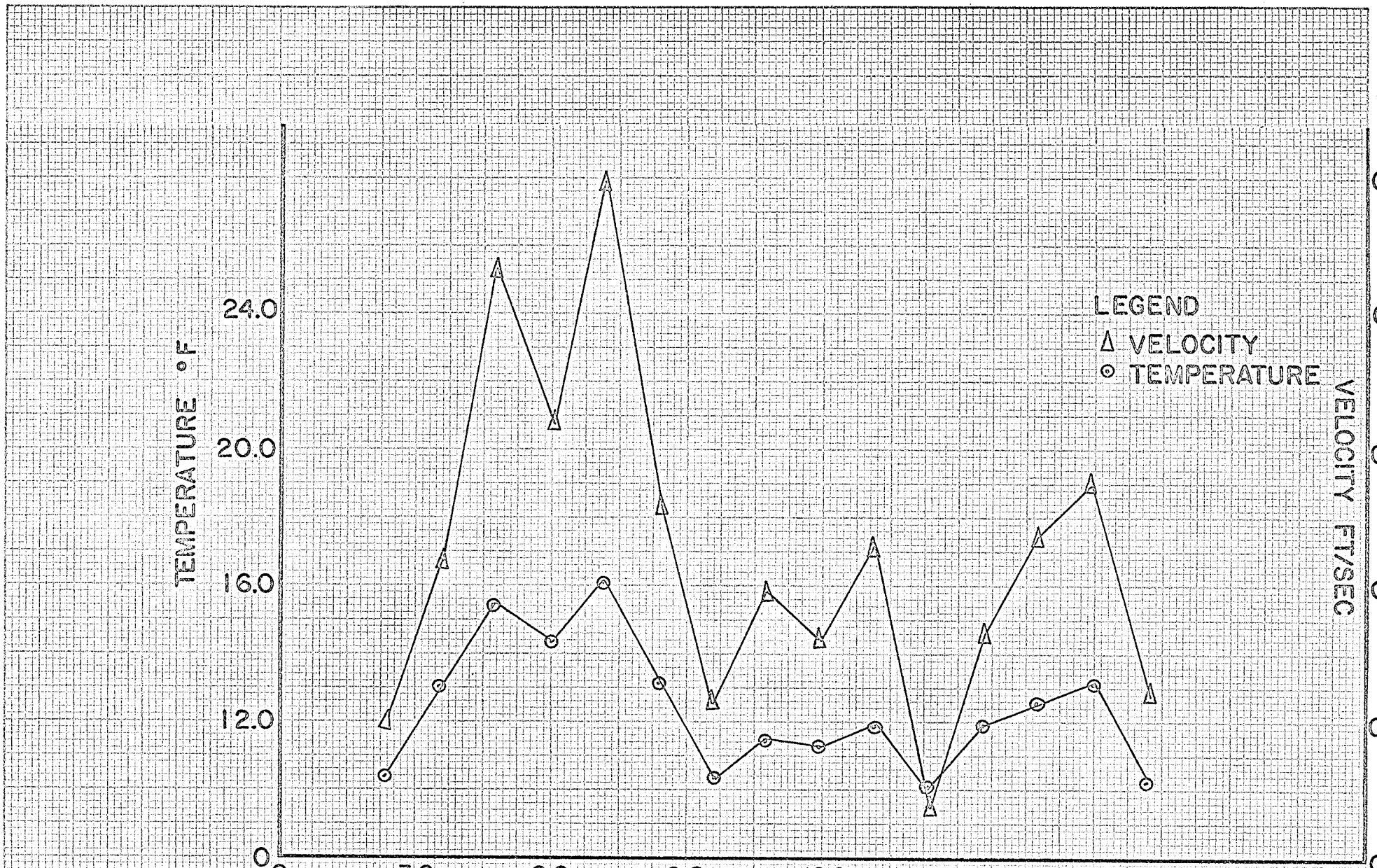

FIGURE 25, VELOCITY PROFILE ABOVE THE HEATER

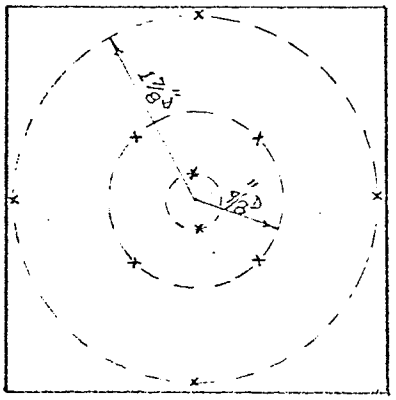

FIG. 26 LOCATION OF THE THERMOCOUPLES ON THE FINS

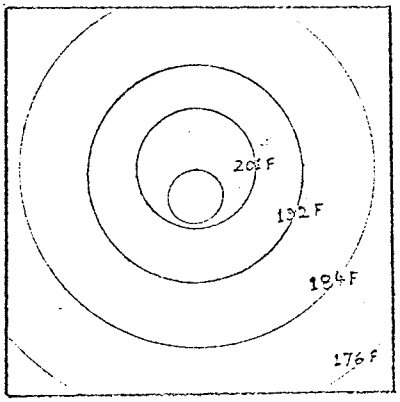

FIG. 27 PREDICTED TEMPERATURE VARIATION ON THE FIN SURFACE

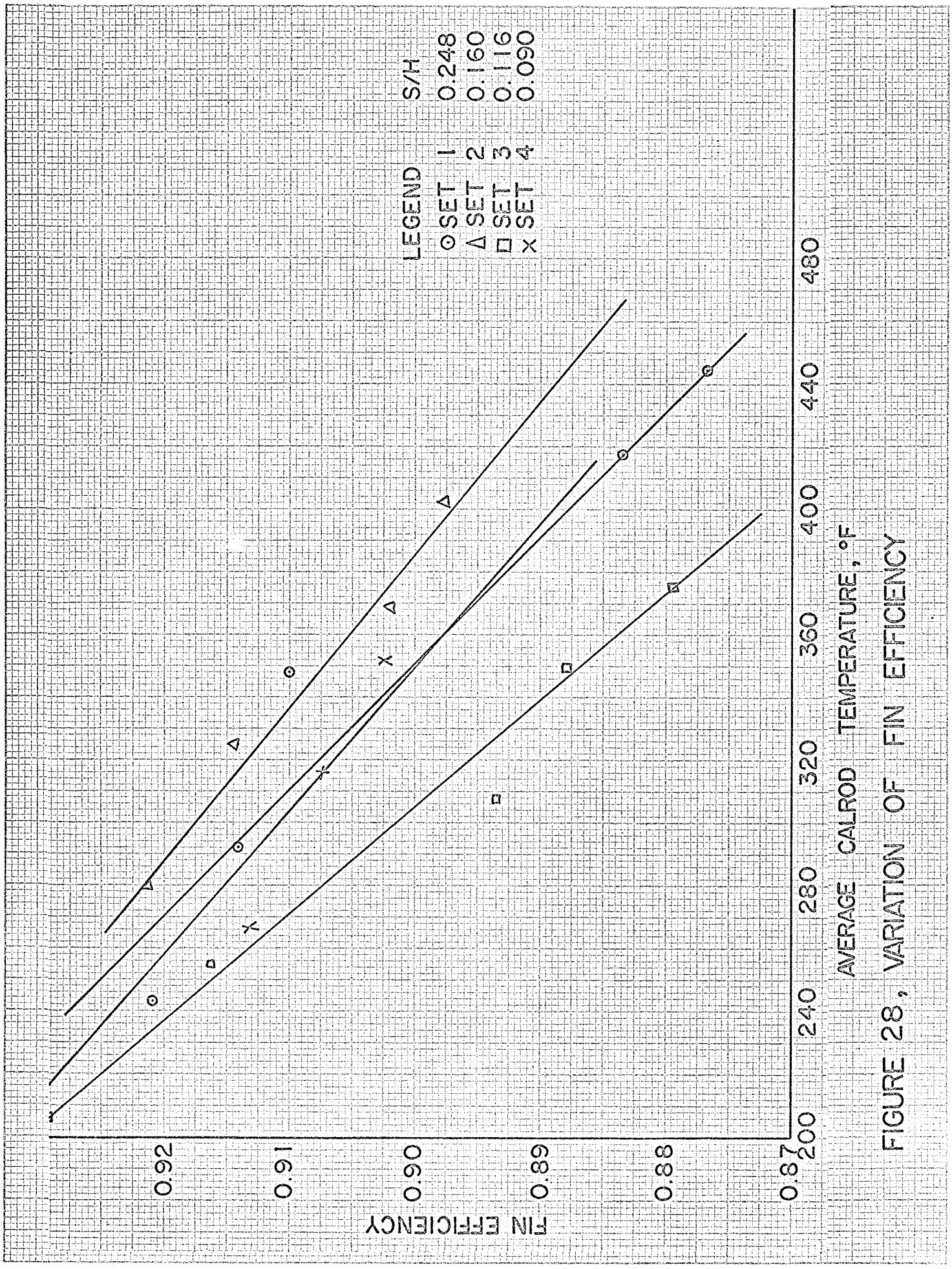

FIGURE 28, VARIATION OF FIN EFFICIENCY

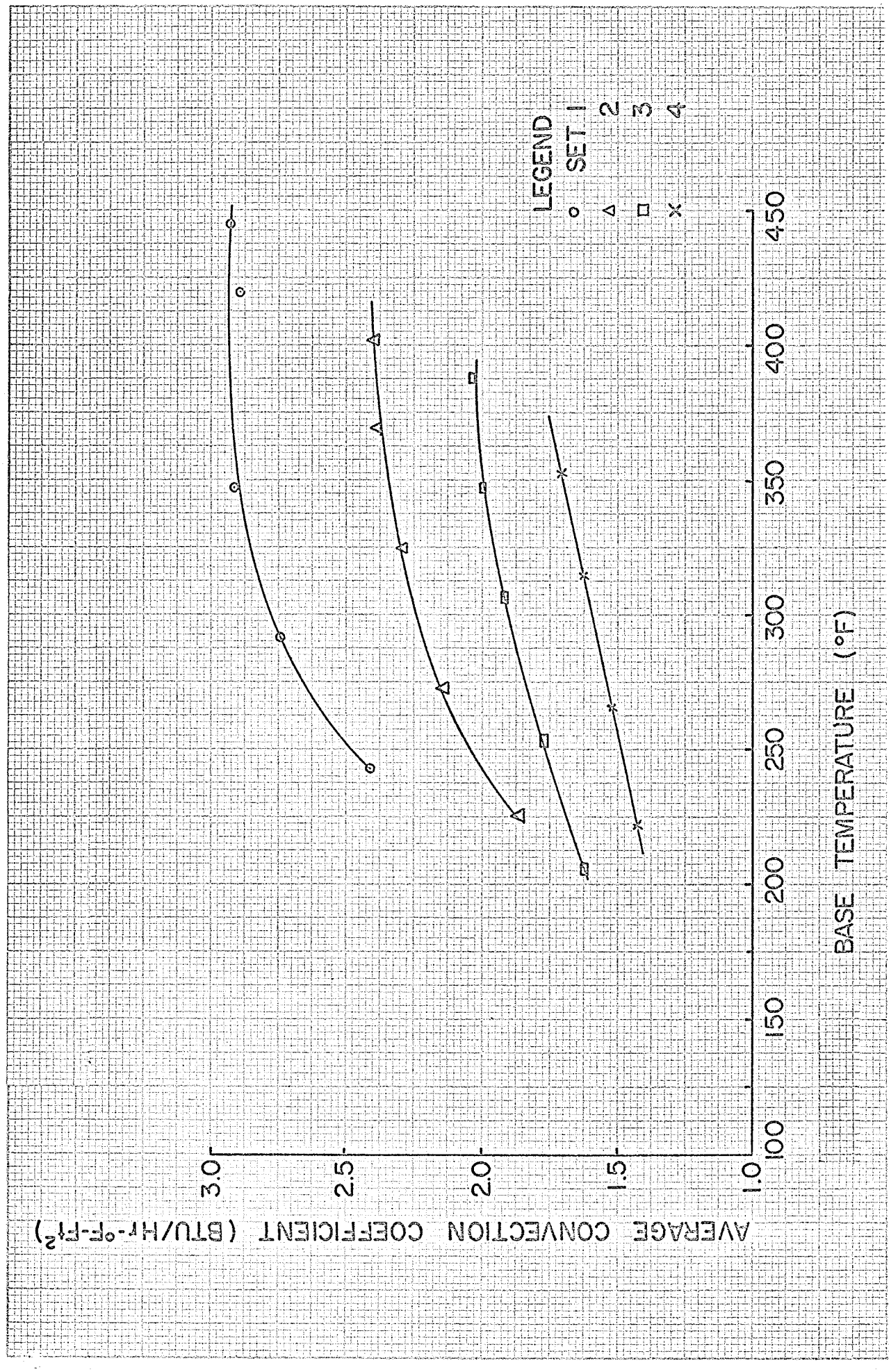

FIGURE 29, VARIATION OF AVERAGE CONVECTION COEFFICIENT

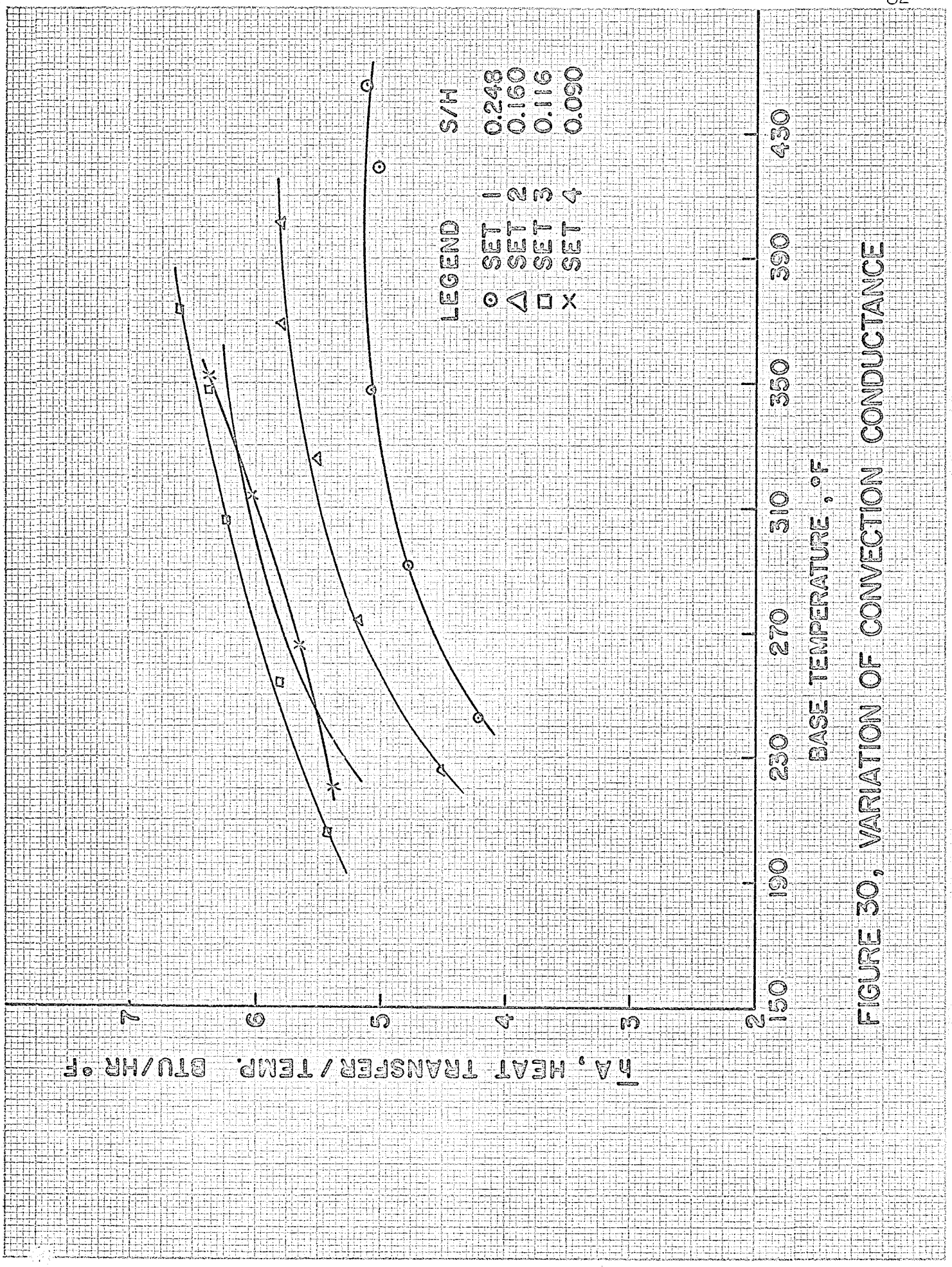

FIGURE 30, VARIATION OF CONVECTION CONDUCTANCE

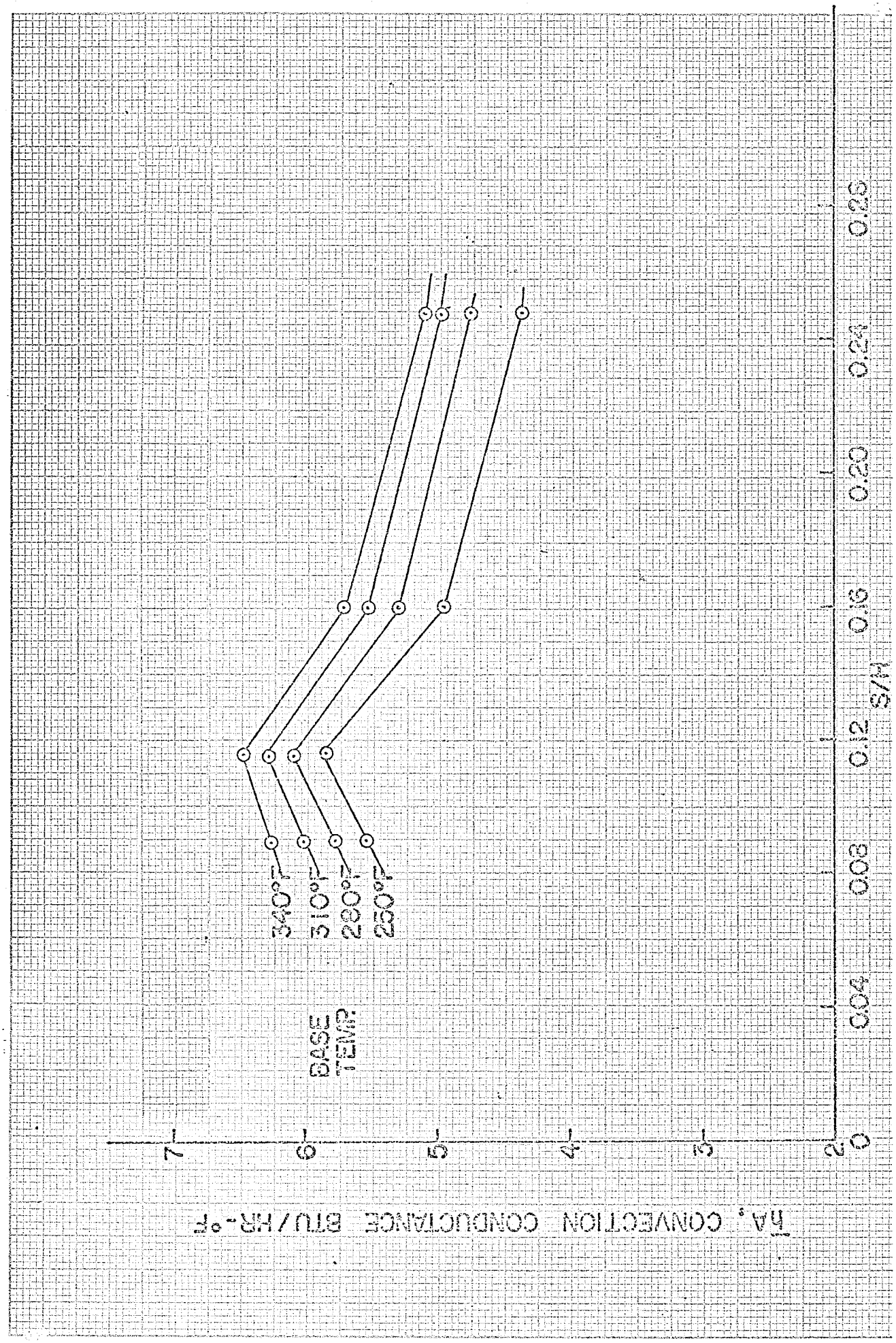

FIGURE 31 VARIATION OF CONVECTION CONDUCTANCE

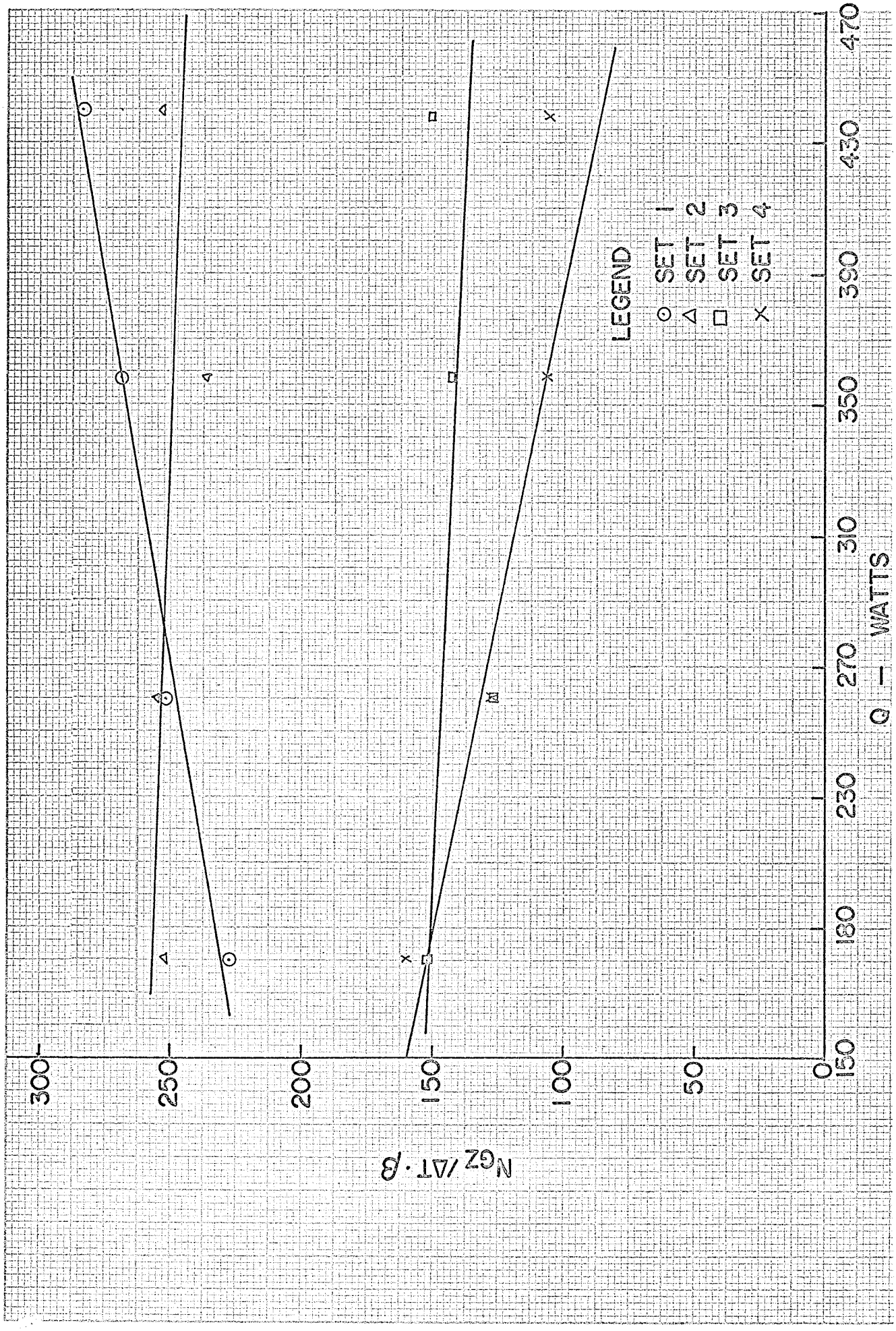

FIGURE 32, VARIATION OF $N_{GZ}/\Delta T \cdot \beta$

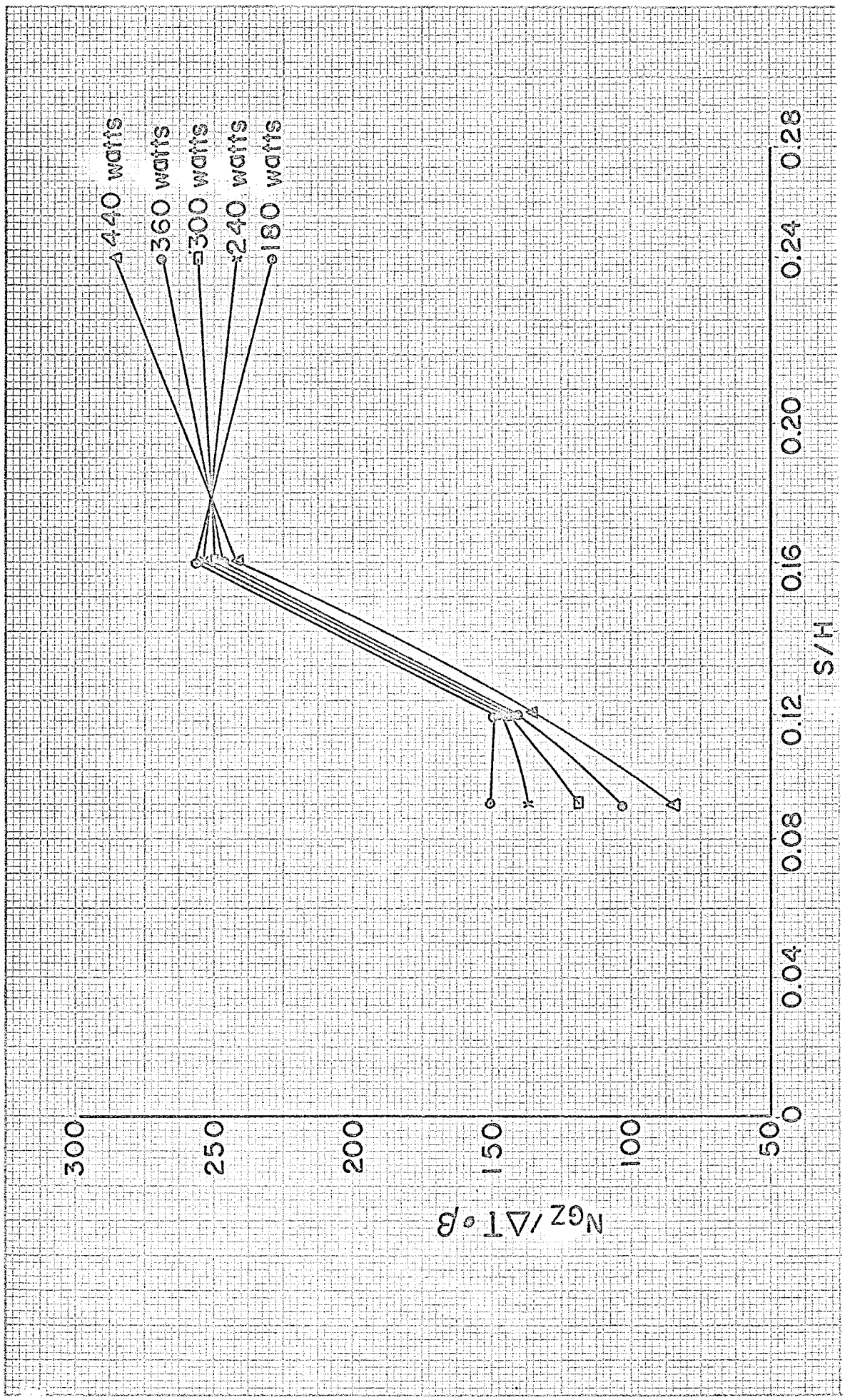

FIGURE 33, VARIATION OF $N_{GZ}/\Delta T \cdot \beta$

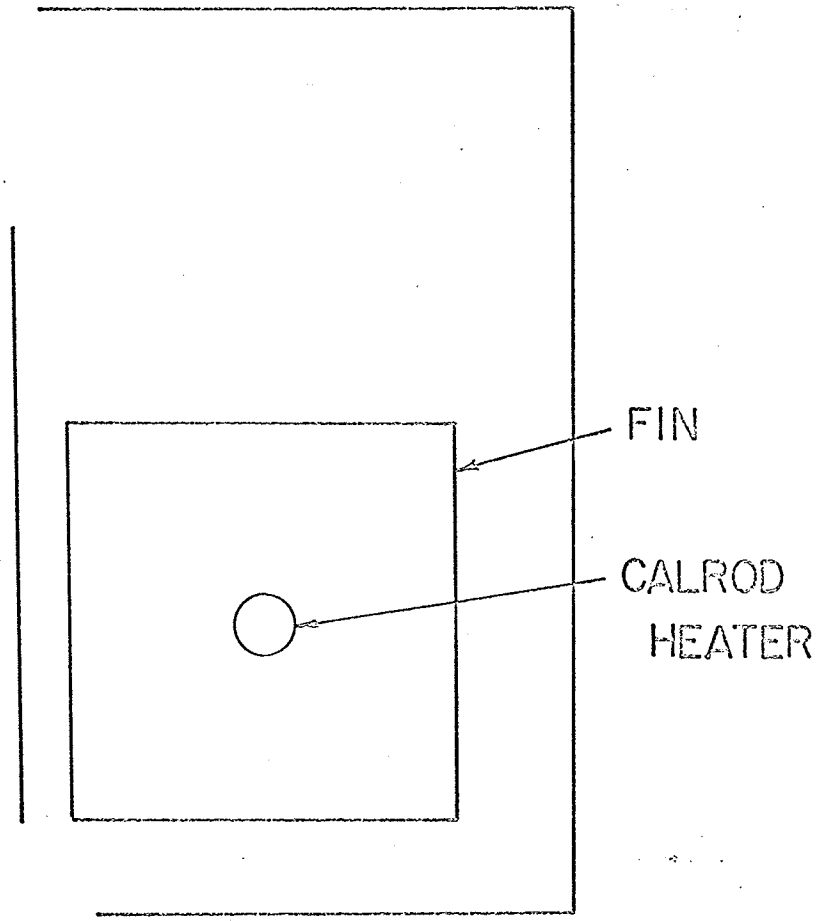

FIGURE 34 HEATER ENCLOSURE NO. 1 (FULL SIZE)

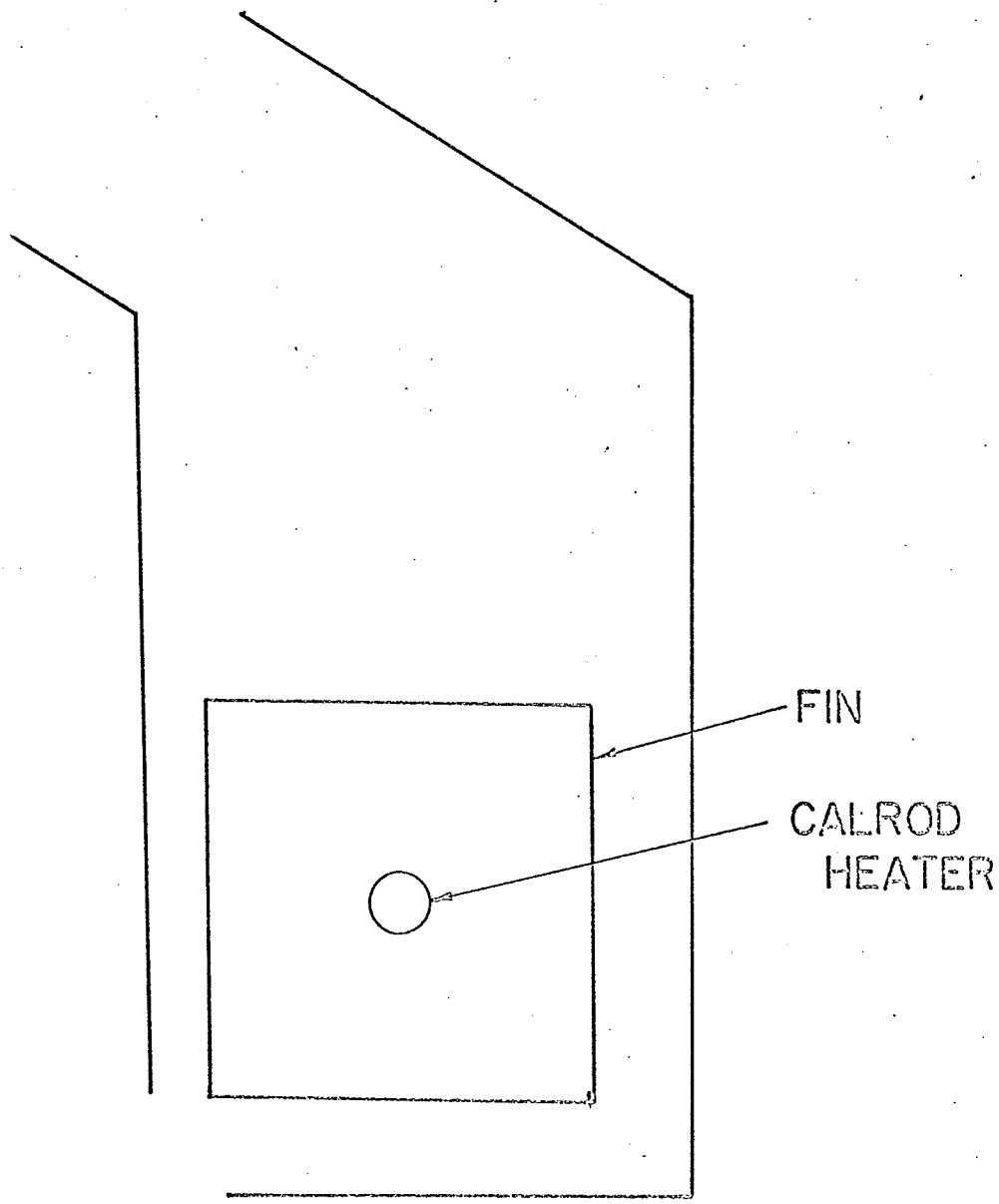

FIGURE 35 HEATER ENCLOSURE NO.2 (FULL SIZE)

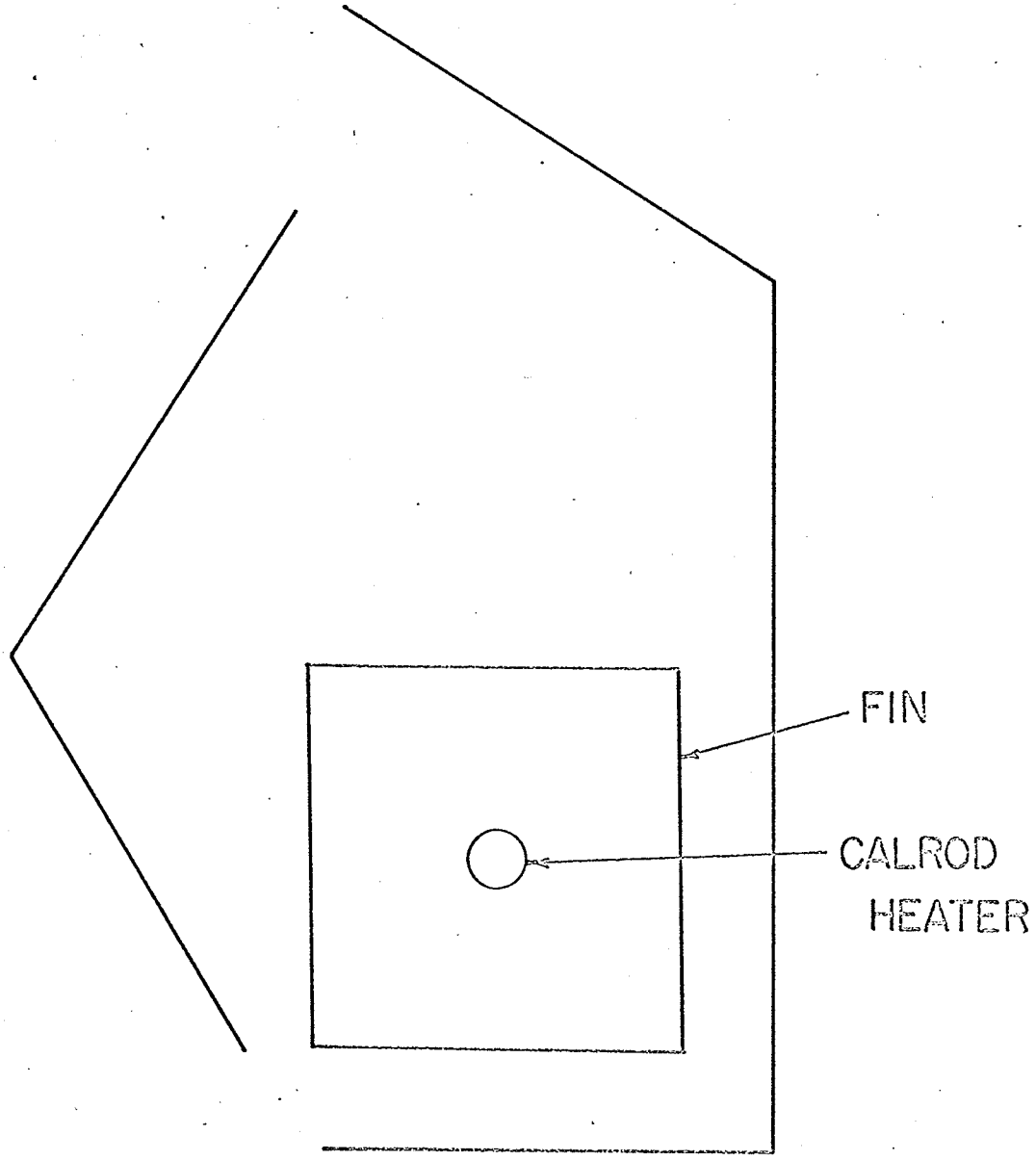

FIGURE 36 HEATER ENCLOSURE NO. 3 (FULL SIZE)

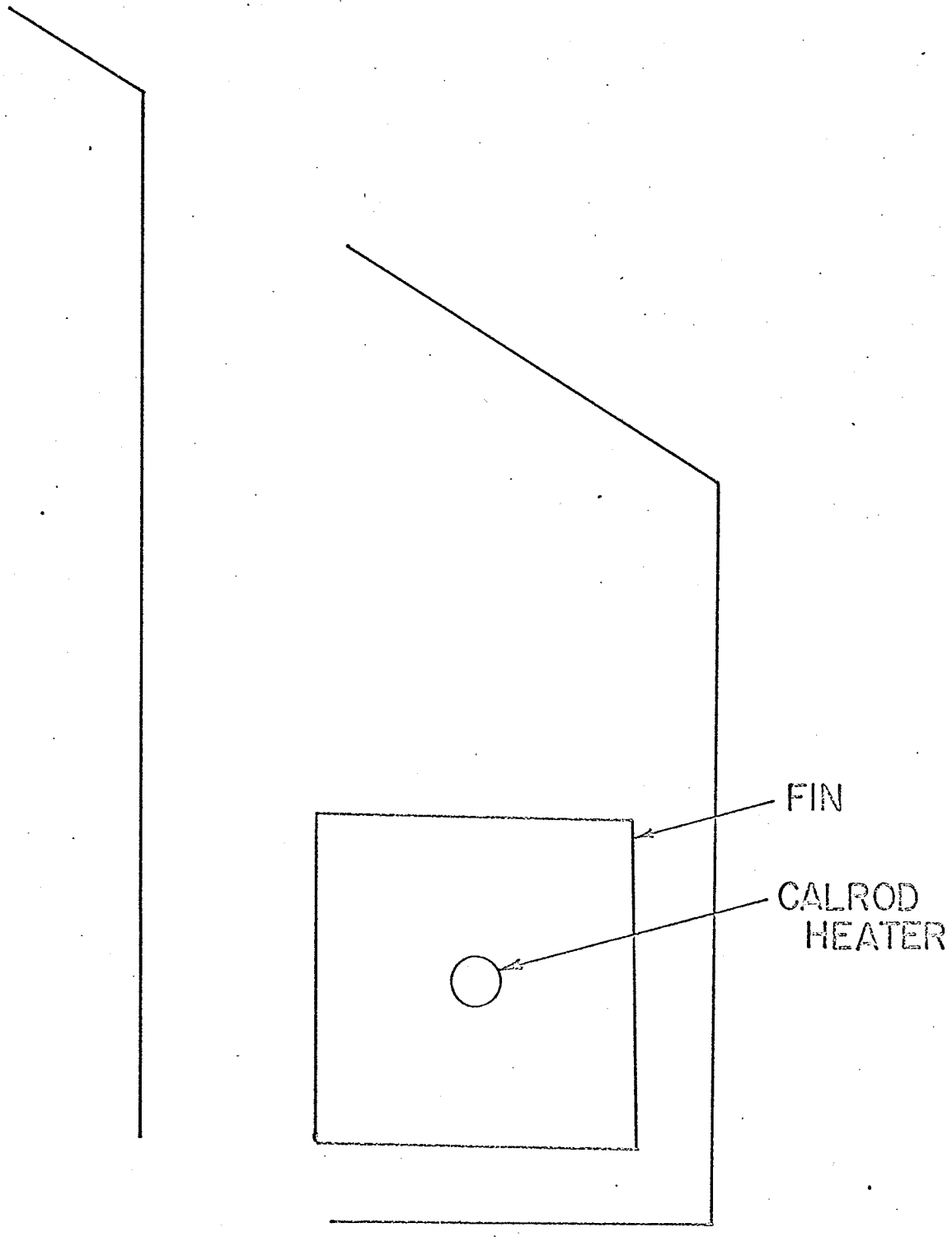

FIGURE 37 HEATER ENCLOSURE NO.4 (FULL SIZE)

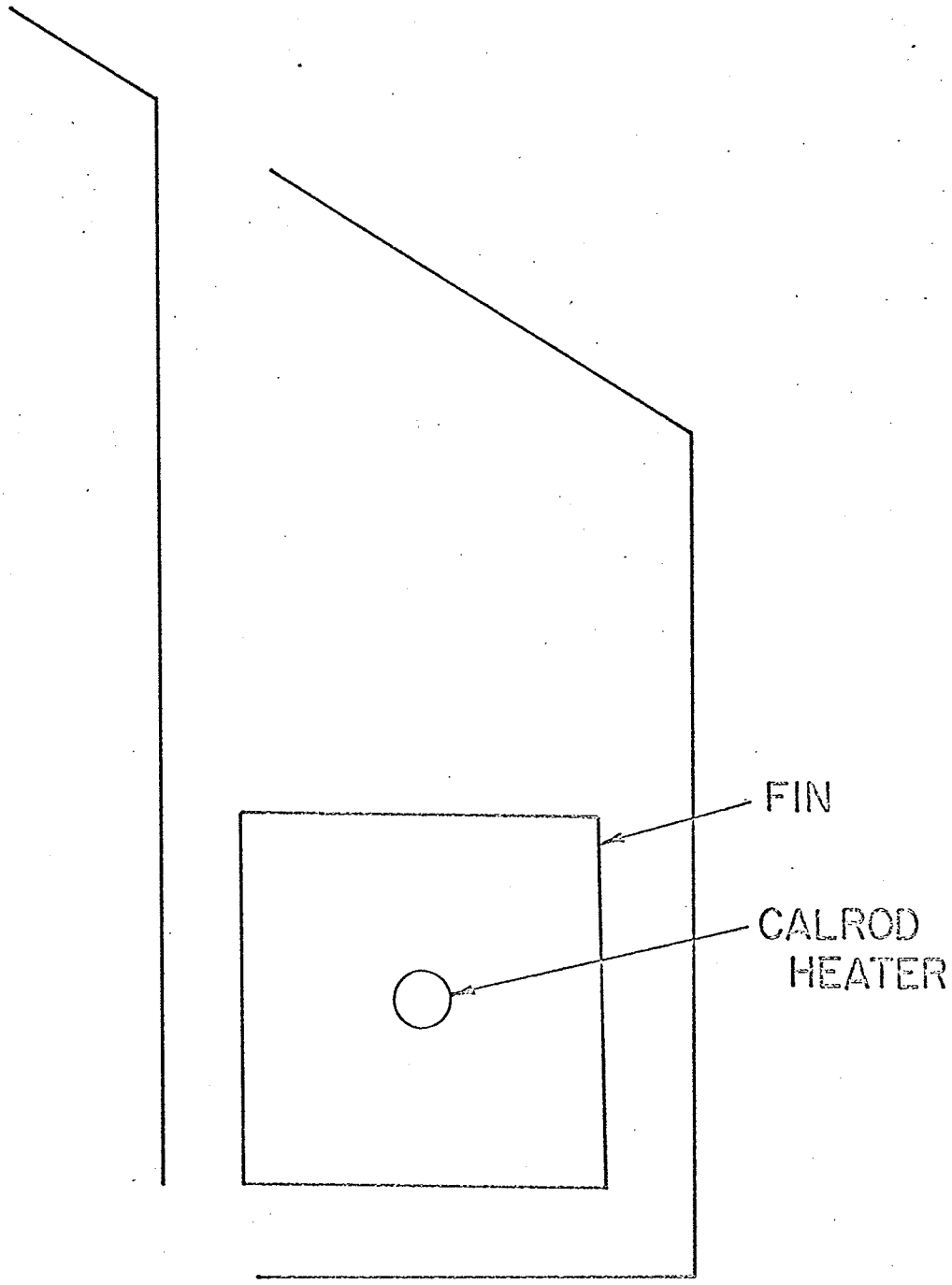

FIGURE 38 HEATER ENCLOSURE NO. 5 (FULL SIZE)

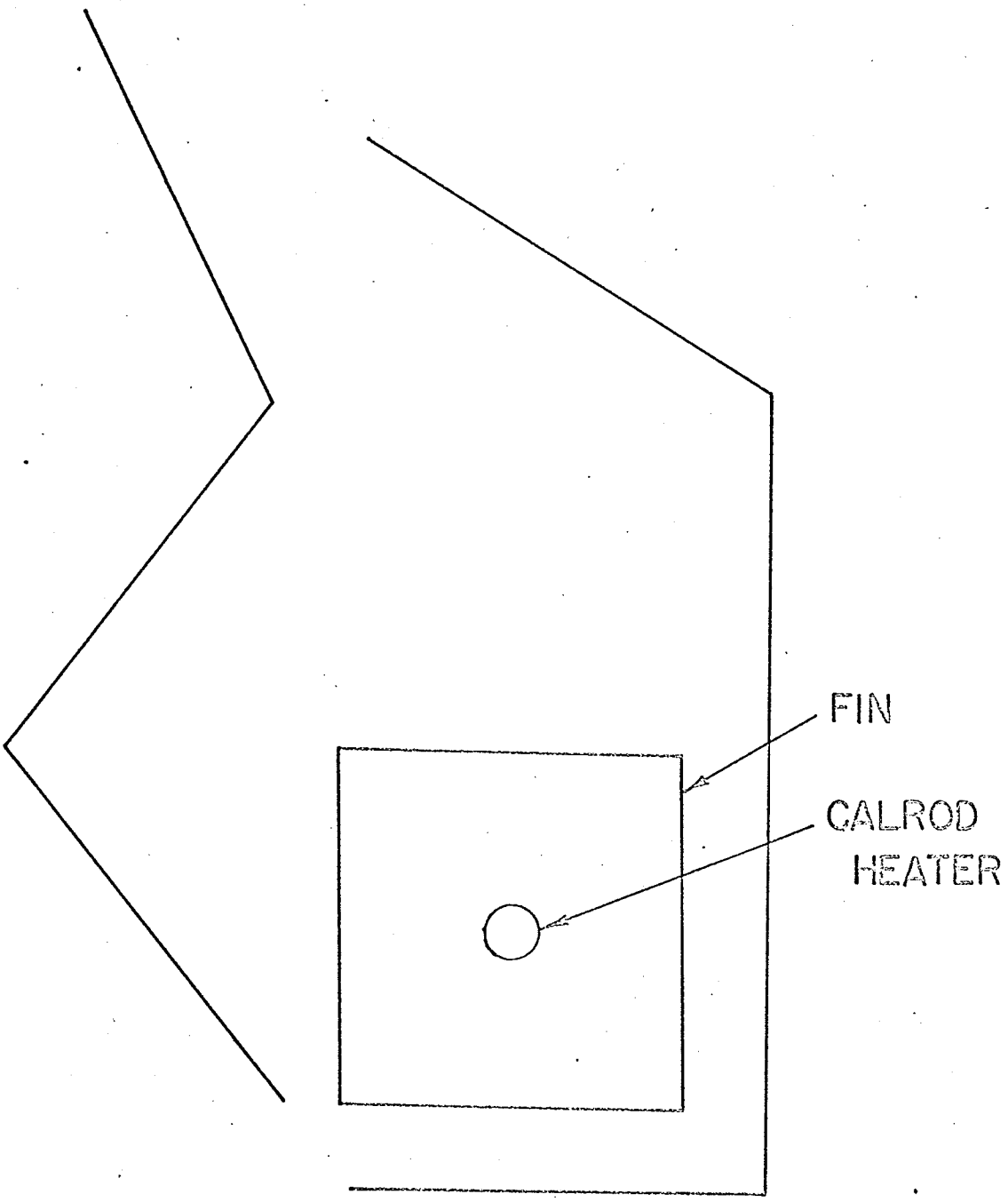

FIGURE 39 HEATER ENCLOSURE NO.6 (FULL SIZE)

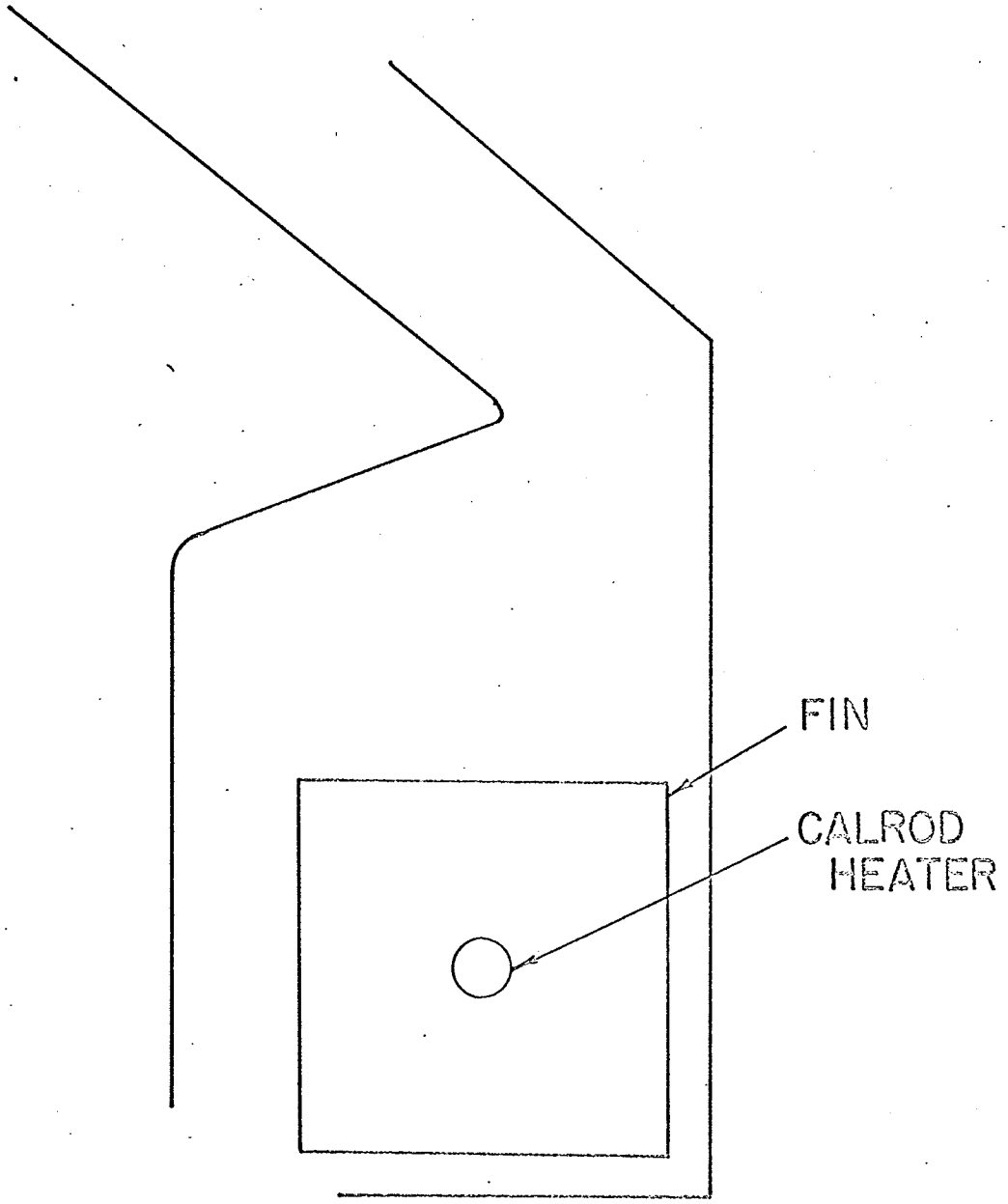

FIGURE 40 HEATER ENCLOSURE NO. 7 (FULL SIZE)

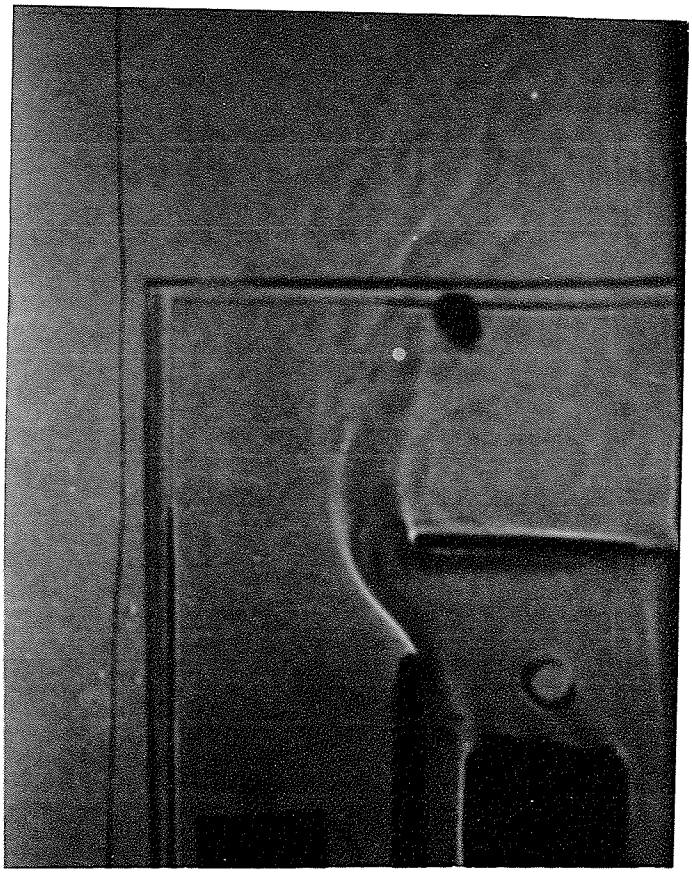

Figure 41. SHADOWGRAPH FOR HEATER ENCLOSURE NO. 1.

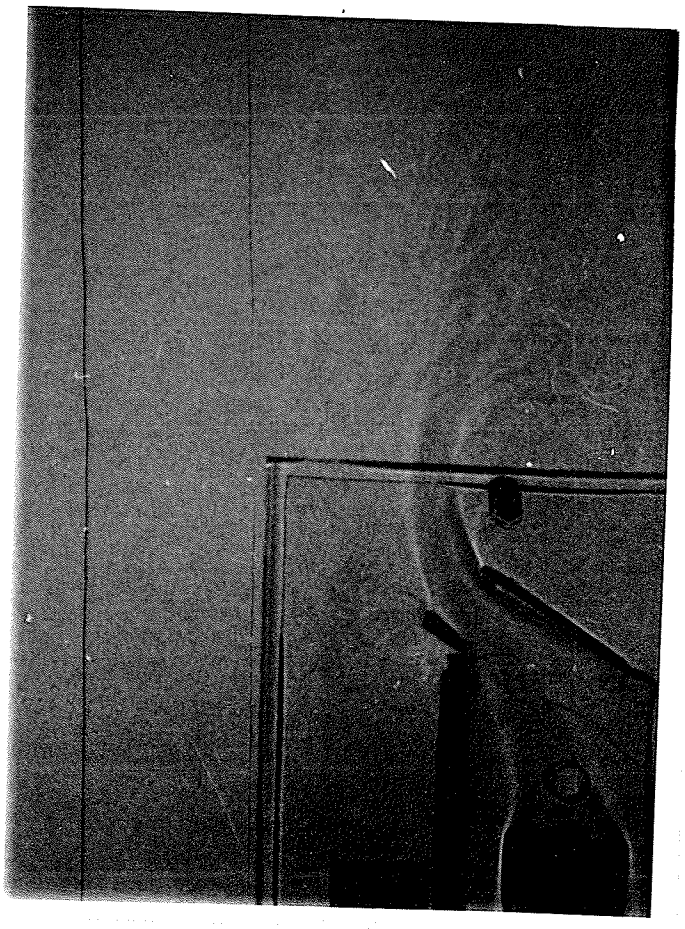

Figure 42. SHADOWGRAPH FOR HEATER ENCLOSURE NO. 2

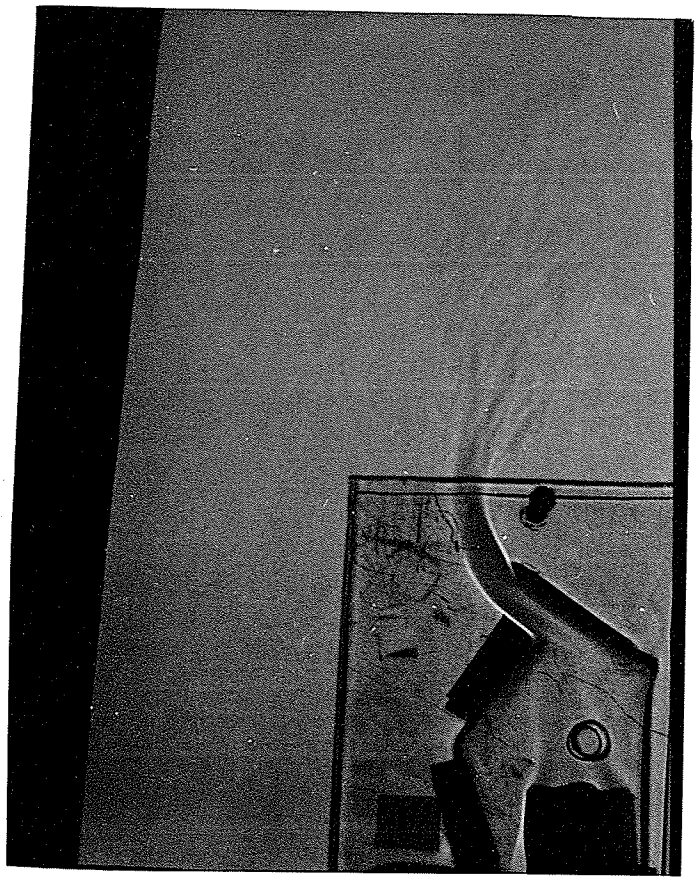

Figure 43. SHADOWGRAPH FOR HEATER ENCLOSURE NO. 4

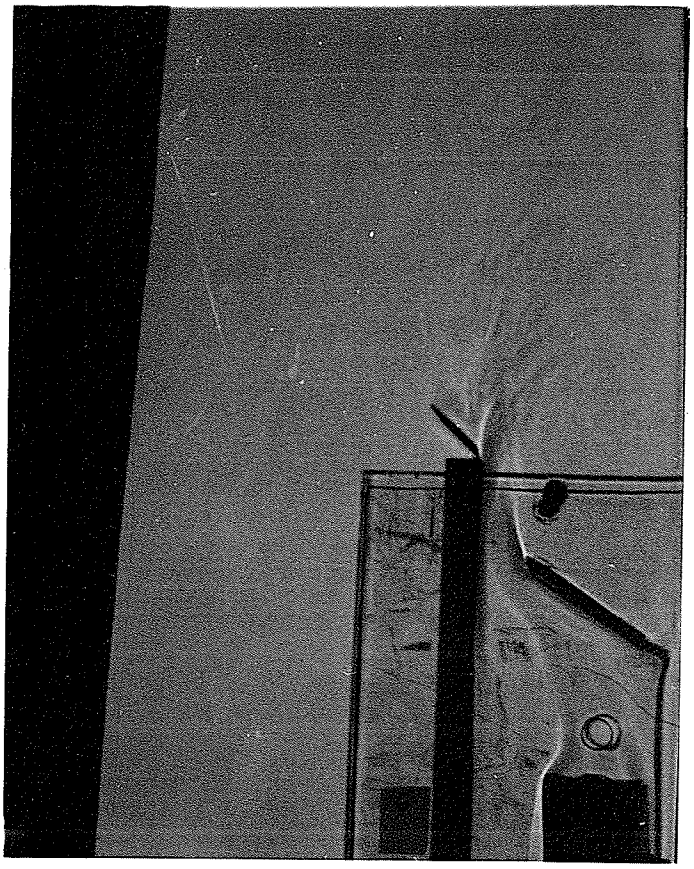

Figure 44. SHADOWGRAPH FOR HEATER ENCLOSURE NO. 5

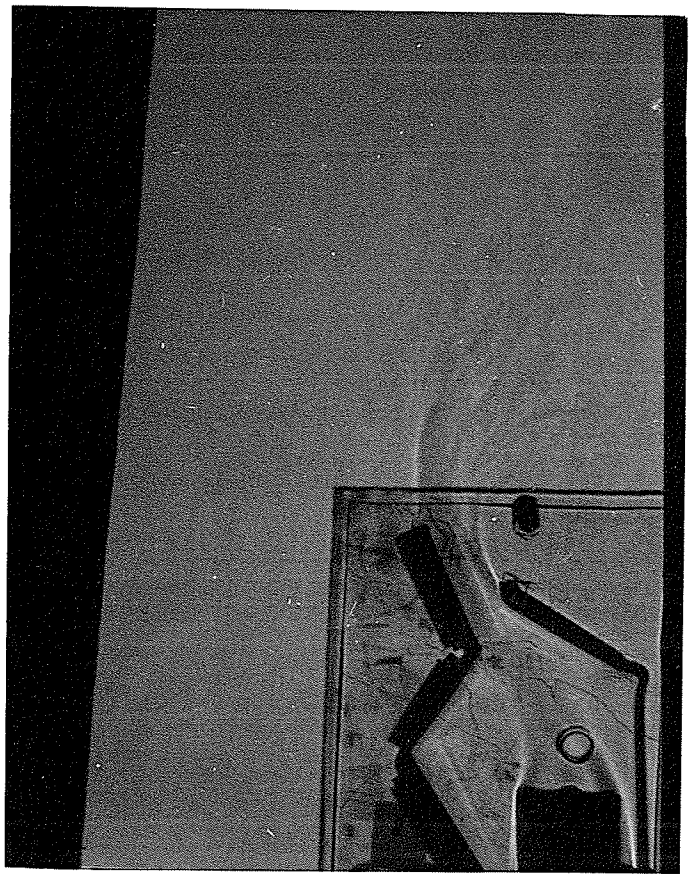

Figure 45. SHADOWGRAPH FOR HEATER ENCLOSURE NO. 6

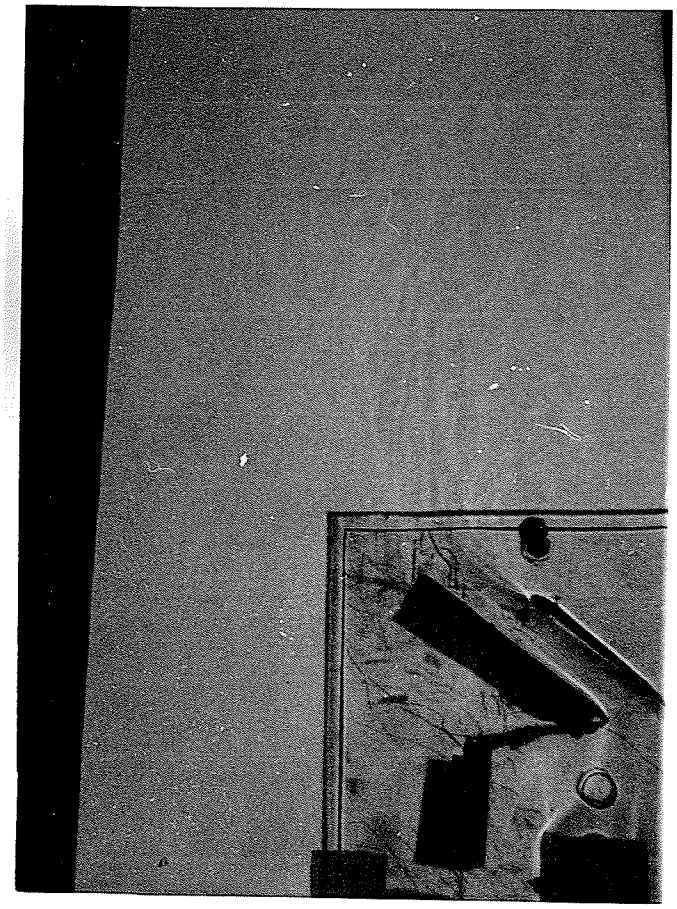

Figure 46. SHADOWGRAPH FOR HEATER ENCLOSURE NO. 7